8-27-2012

Peridynamic constitutive model for concrete

Bhanu Kiran Tuniki

Bhanu Kiran Tuniki
Candidate

Civil Engineering
Department

This thesis is approved, and it is acceptable in quality and form for publication:

Approved by the Thesis Committee:

Dr. Walter H. Gerstle , Chairperson

Dr. Timothy J. Ross

Dr. Percy Ng

PERIDYNAMIC CONSTITUTIVE MODEL
FOR
CONCRETE

by

BHANU KIRAN TUNIKI

B.E. CIVIL ENGINEERING, OSMANIA UNIVERSITY
2008

THESIS

Submitted in Partial Fulfillment of the
Requirements for the Degree of

Master of Science

Civil Engineering

The University of New Mexico
Albuquerque, New Mexico

July, 2012

DEDICATION

To my parents who supported me in every part of my life.

ACKNOWLEDGEMENTS

Foremost, I would like to express my sincere gratitude to my advisor Prof. Dr. Walter Gerstle for the continuous support of my Master's study and research, for his patience, motivation, encouragement, and supporting me financially through research assistantship. His advisement helped me all the time of this research and in writing my thesis. I could not have imagined having a better advisor for my Master's study. His guidance throughout my study at The University of New Mexico has been invaluable, and will remain within me throughout my career.

I would like to thank my thesis committee members Dr. Timothy J. Ross and Dr. Percy Ng for their comments and suggestions.

I would like to thank Center for Advanced Research Computing for the use of facilities and supercomputing cluster. I also would like to thank my friend Hossein Honarvar Gheitenbaf for this help with the development of required code for implementing the concrete model in pdQ.

Lastly, I would like to thank for my parents, friends, and family members for their love and support to me.

Peridynamic Constitutive Model for Concrete

By

Bhanu Kiran Tuniki

B.E., Civil Engineering, Osmania University, 2008

M.S., Civil Engineering, University of New Mexico, 2012

Abstract:

Peridynamics, as originally proposed by Silling in 1998, is a spatio-temporal integral reformulation of the classical partial differential equations of motion. In contrast with the classical theory, the concepts of stress and strain are not needed in peridynamics. The original bond-based peridynamic theory has several drawbacks including being limited to modeling materials with Poisson's ratio of one-quarter. In 2007, Silling generalized his model by introducing state-based peridynamics. Sau et al. proposed a micropolar model for concrete in 2007, but were unable to fully implement the model. In 2011, Sakhavand developed software called pdQ that is capable of modeling micropolar peridynamics. While he did model concrete using the bond-based peridynamic theory, he did not attempt to model concrete using micropolar peridynamics. In 2011 Rahman developed a micropolar peridynamic model with hexagonal particle lattice. Rahman studied only linear elastic problems with this model.

In this thesis, we propose a new micropolar peridynamic lattice-based damage model for concrete. The model is implemented in pdQ. This model is state-based, in that the force acting between two particles no longer depends only on the states of the two particles, but it also depends on the states of other neighboring particles.

We obtained appropriate parameters for a micropolar, lattice-based, and state-based constitutive model for the concrete. Example problems, including uniaxial tension, uniaxial compression, and confined compression are considered. Known features, including elasticity, damage, and fracture, of concrete appear to be well-replicated by the new model. Also other example problems are solved to demonstrate the versatility of the new model.

TABLE OF CONTENTS

LIST OF FIGURES X

1. INTRODUCTION 1

1.1 Peridynamic Modeling 2

1.2 pdQ Software 2

1.3 Objective of Thesis 3

1.4 Scope of Thesis 3

2. LITERATURE REVIEW 6

2.1 Peridynamic Model 6

2.2 Micropolar Model 9

2.3 Lattice Models 14

2.4 Concrete Models 15

2.5 Dynamic Relaxation Method 18

3. PERIDYNAMIC MODEL FOR CONCRETE 20

4. CALIBRATION OF PERIDYNAMIC PARAMETERS 25

3.1 Concrete in Uniaxial Tension 25

3.2 Concrete in Uniaxial Compression 32

3.3 Concrete in Confined Compression 38

5. EXAMPLES 41

5.1 Dynamic Effects 41

5.2 Simply Supported Unreinforced Concrete Beam 43

5.3 Simply Supported Reinforced Concrete Beam 46

5.4 Unreinforced Cantilever Concrete Beam 48

5.5 Reinforced Cantilever Concrete Beam 51

5.6 Deep Beam 54

6. CONCLUSIONS 56

6.1 Summary and Conclusions 56

6.2 Future work 58

7. REFERENCES 59

LIST OF FIGURES

Fig. 2.1 Terminology of Peridynamic model 7

Fig. 2.2 Constitutive Behavior of a Micropolar Peridynamic Link for Concrete 11

Fig 2.3 Peridynamic link for 2D 12

Fig 2.4 Degrees of freedoms for 2D link for linear elastic MPM 13

Fig. 2.5 Triangular truss (using bar elements) used by Hrennikoff 14

Fig 2.6 2D Lattice with six neighboring particles 16

Fig 2.7 3D Lattice with 18 neighboring particles 16

Fig 2.7 (a) Undamped oscillations 19

Fig 2.7 (b) Damped oscillations 19

Fig. 3.1 – 2D hexagonal lattice of particles 20

Fig. 3.2 Modified micropolar model for concrete 21

Fig. 3.3 Peridynamic link with degrees of freedom shown 22

Fig. 4.1 Concrete plate 15” x 45” x 1” modeled for calibration 26

Fig. 4.2 Time history plot of concrete plate loaded in tension 27

Fig. 4.3 Deformed shape of concrete plate in tension 28

Fig. 4.4 Deformed shape of concrete plate with tension cracks 29

Fig. 4.5 Time history plot of concrete plate loaded in tension 30

Fig. 4.6 Concrete specimen failed in compression test.....33

Fig. 4.7 Time history plot of concrete plate loaded in compression.....33

Fig. 4.8 Deformed shape of concrete plate in compression.....34

Fig. 4.9 Time history plot of concrete plate loaded in compression.....35

Fig. 4.10 Deformed shape of concrete plate with failed in compression.....35

Fig. 4.11 Concrete plate 15” x 46” with confined boundaries.....39

Fig. 4.12 Deformed concrete plate 15” x 46” with confined boundaries 39

Fig 5.1 Concrete Plate under uniaxial tension with rampforce for time T 41

Fig 5.2 Concrete Plate under uniaxial tension with rampforce for time 2.0T 42

Fig. 5.3 Description of Simply supported beam 43

Fig. 5.4 Deformed shape of simply supported beam at

(a) 8000 and (b) 9000 time steps.....45

Fig. 5.5 Description of Simply supported reinforced concrete beam 46

Fig. 5.6 Deformed shape of reinforced simply supported

at (a) 45,000 and (b) 50,000 time steps.....47

Fig. 5.7 Close view of the cracks shown in Fig 5.6 (b) 48

Fig. 5.8 Description of unreinforced cantilever concrete beam.....49

Fig. 5.9 Deformed shape of unreinforced cantilever beam.....50

Fig. 5.10 Description of reinforced cantilever concrete beam.....51

Fig. 5.11 Deformed shape of reinforced cantilever beam.....53

Fig. 5.12 Description of unreinforced concrete deep beam.....54

Fig. 5.13 Deformed shape of unreinforced concrete deep beam 55

Fig. 6.1 Modified micropolar model for concrete.....57

Chapter 1. Introduction

Concrete is an important building material. By accurately modeling concrete, we can utilize its full strength, thus saving material in civil engineering structures. This saves money and increases safety. Several models have been proposed for concrete, but none of these models has proven fully effective for modeling fracture and damage.

Though continuum mechanics and finite element methods have been applied to materials like concrete, they have limited application when modeling material damage. With damage, the basic assumption of displacement continuity is usually not valid.

Researchers have applied fracture mechanics methods to model concrete. The smeared crack approach and the discrete crack approach have been used to model damage. In smeared crack models, the cracks are represented through changes of the material constitutive equations. The dependency of the results on mesh refinement is the major deficiency with smeared crack models [Nguyen and Chun 2005]. The discrete crack approach [Cervenka et al. 2001] is directly based upon the principles of linear elastic fracture mechanics (LEFM) or upon the cohesive crack model. This method is more suitable to capture failure localization, but requires redefinition of the geometry and re-meshing to account for progressive crack propagation. To overcome these limitations, new methods need to be developed that can more effectively model quasi-brittle materials like concrete.

1.1 Peridynamic Modeling

In an effort to overcome the limitations of classical continuum and fracture mechanics, the peridynamic model was proposed by Silling [Silling 1998]. The term 'peridynamic' is derived from the Greek words 'near' and 'force'. Silling's peridynamic equations do not assume spatial differentiability of the displacement field, and permit displacement discontinuities to arise as part of the solution. The peridynamic theory is non-local, locality is recovered as a special case, and peridynamics can be thought of as a generalization of the classical theory of elasticity.

The peridynamic method uses spatial integral equations to compute the forces acting upon the particles. The particle positions are integrated in time, based upon these evolving forces. This is an effective method for modeling damage, which classical theories fail to efficaciously model. The applicability of peridynamic equations at all points within the model avoids special cases at discontinuities in the displacement field. For example, in peridynamics, there is no need for a separate crack growth law based on a stress intensity factor.

1.2 pdQ Software

Recently, Atlas, Sakhavand and Gerstle developed particle simulation software called pdQ [Sakhavand 2011]. This software is used throughout this research. Preprocessing and postprocessing of the simulations are implemented using Matlab. Simulations employ high-performance parallel computers. Honarvar recently updated pdQ to allow for micropolar state-based peridynamic modeling of solids. On 32-processor computers, simulations with one million particles are reasonable, and the solution time is approximately inversely proportional to the number of processors.

In this thesis, the pdQ software is used to implement the lattice-based micropolar model for concrete. The dynamic relaxation method, with artificial enhanced damping is used to achieve the steady state static solution.

1.3 Objective of Thesis

The objective of this thesis is to develop a new working damage model for concrete. For this purpose we start with the micropolar peridynamic model proposed by Sau [Sau 2007]. We have modified this micropolar model with damage parameters with a new pairwise force function. This new micropolar model is implemented in conjunction with the lattice-based peridynamic method developed by Rahman [Rahman 2012]. This method is used to model many of the known features of concrete including elasticity, damage, and fracture. This model is verified by solving various example problems.

1.4 Scope of Thesis

In this research, various concrete models have been studied and the micropolar model proposed by Sau [Sau 2007] is used as a starting point to implement lattice-based, state-based, micropolar peridynamics. Latticed-based peridynamics, proposed by Rahman [Rahman 2012] is shown to have less severe boundary effects than the original implementation of peridynamics. Lattice-based peridynamics, with material horizon slightly larger than the particle spacing, reduces the number of particle interactions required.

This thesis is divided into six chapters: Introduction, Literature Review, Peridynamic Model for Concrete, Calibration of Peridynamic Parameters, Examples, and Conclusions.

Chapter Two is the literature review, divided into five sections. The first section introduces the theory of peridynamics. In the second section, the micropolar model proposed by Sau is discussed. In the third section, various lattice models are discussed and lattice-based peridynamics is studied. In the fourth section, various concrete models that have been proposed by other researchers are discussed. In the fifth section, the dynamic relaxation method is discussed.

Chapter Three explains the new micropolar model that is proposed in this study to model damage of the concrete. In this chapter, a brief description of the original peridynamic discretization method (which assumes an infinite number of particles in R3 space) is first presented to explain why we have adopted the lattice model instead.

In Chapter Four, the parameters of the micropolar model proposed in the Chapter Three are calibrated for a typical concrete. This chapter is divided into three sections. In the first section, concrete material model properties are calibrated for uniaxial tension, in second section concrete material model parameters are calibrated for uniaxial compression, and in the third section concrete properties are verified for confined compression.

In Chapter Five some example problems are simulated to verify the model. These example problems include a simply supported beam with and without tension reinforcement, Cantilever beam with and without tension reinforcement. These problem

have demonstrated the capabilities of the concrete model that has been presented in Chapter Three.

The last chapter summarizes the work done in this thesis, draws conclusions and suggests future work to improve the model. And the list of references that are studied during this research are presented at the end.

Chapter 2. Literature Review

Continuum mechanics fails to adequately model cracking. The limitations of continuum mechanics are partially addressed by the field of the fracture mechanics, but fracture mechanics has its own limitations

The peridynamic model has advantages for modeling damage in solids. In this model, the structure is thought of as a collection of discrete particles with inter-particle force functions called peridynamic forces. The forces and displacements acting upon each particle are computed using integration. The basic equations can be applied anywhere in the model including at the cracks, so no additional theories are necessary for studying damage and cracking using peridynamics.

2.1 Peridynamic Model

No assumptions, such as of small deformations or of material continuity, need to be made in peridynamics. Discontinuities and cracks emerge with the peridynamic solution. Materials are modeled through the inter-particle force functions. In peridynamics, the motions of particles are assumed to follow Newton's second law.

The maximum interaction distance between particles in peridynamics is termed the "material horizon (δ)". When the distance between two particles is less than or equal to material horizon then they potentially interact and the pairwise force between them is a specified function that depends (in the original bond-based theory) upon both initial and the deformed positions of the two particles. [Silling 1998].

Referring to the Fig. 2.1, at any point $\underline{x}_i$ in the reference configuration, R, and at time t, the force $\underline{L}$ ($\underline{x}_i$, t) that all particles $\underline{x}_j$ exert on $\underline{x}_i$ is given by:

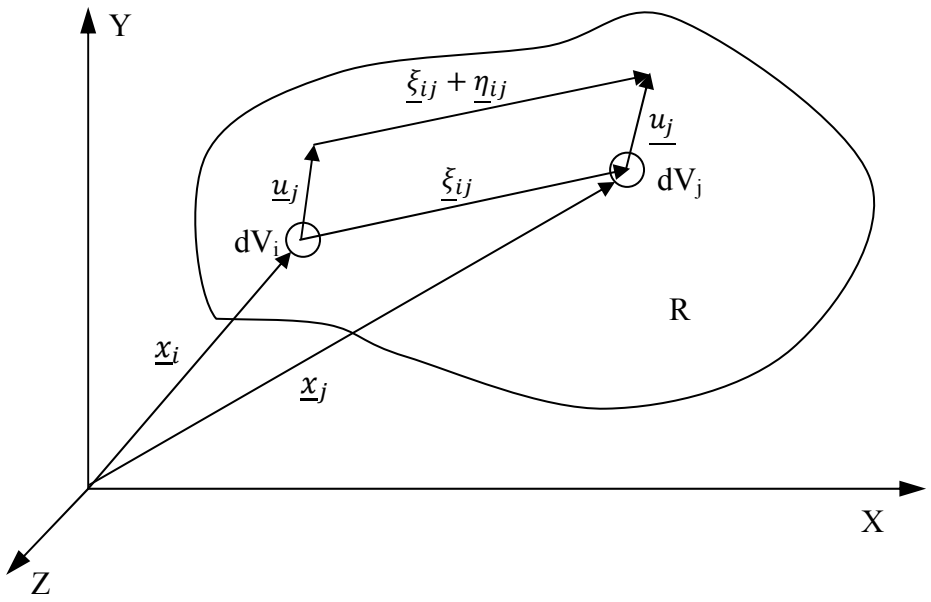

Fig 2.1 Terminology of Peridynamic model.

$$\underline{L}\,(\underline{x},\,\mathrm{t}) = \int_R \underline{f}\big(\underline{u}(\underline{x}_j,\ t) - \underline{u}(\underline{x}_i, t),\ \underline{x}_j - \underline{x}_i\big)dV_j \quad \forall\ \underline{x} \in \mathrm{R},\ \ \mathrm{t} \geq 0 \qquad (2.1)$$

where $\underline{L}$ is the pair wise force (per unit volume) acting upon $\underline{x}_i$ due to all particles $\underline{x}_j$, $\underline{u}$ is the displacement field, and $\underline{x}_i$ is a point anywhere in the region R. The underscore indicates a physical vector quantity. $\underline{f}$ is the pairwise force (per unit volume squared) acting between particles i and j.

More concisely,

$$\underline{L}(\underline{x}_i) = \int_H \underline{f}\left(\underline{u}_j - \underline{u}_i,\ \underline{x}_j - x_i\right) dV_j \quad \forall \quad \underline{x}_i, \underline{x}_j \in \text{ H}, \quad t \geq 0 \tag{2.2}$$

Where H is the region including $\left|\underline{x}_i - \underline{x}_j\right| < \delta$.

The peridynamic vector equation of motion is given by

$$\rho \underline{u} = \underline{L} + \underline{b}, \tag{2.3}$$

where $\underline{b}$ is the external force per unit reference volume, and ρ is the material density.

For static conditions, the peridynamic equilibrium equation is given by

$$\underline{L} + \underline{b} = 0 \quad \text{or} \int_H \underline{f}\ \left(\underline{\eta}, \underline{\xi}, \underline{\theta}\right) dV_j + \underline{b}_i = 0 \tag{2.4}$$

where $\underline{\eta} = \underline{u}_j - \underline{u}_i$ and $\underline{\xi} = \underline{x}_j - \underline{x}_i$ are the relative displacement and relative position vectors.

For a bond-based peridynamic linear elastic material, the pairwise force function, $\underline{f}$, is represented as [Silling 1998, Gerstle et al. 2005],

$$\underline{f}\ \left(\underline{\eta}, \underline{\xi}\right) = c\left(\frac{\left|\underline{\xi}+\underline{\eta}\right| - \left|\underline{\xi}\right|}{\left|\underline{\xi}\right|}\right) = c\ s \tag{2.5}$$

where $\underline{f}$ has units of force per unit volume squared, c is called the peridynamic microelastic constant and s is the stretch of the peridynamic link.

In this model, Silling assumes that the force between two particles depends only on the relative positions (current and reference) of two particles. The original

implementation of the peridynamic method (in EMU) was for a cubic arrangement of particles with the material horizon being three times the spacing of the particles. With this method, in 3D problems each particle potentially interacts with 106 other particles. In the current lattice-based state-based peridynamic method the material horizon is slightly greater than the particle spacing reducing the number of particle interactions to 18 in 3D, or 6 in 2D, or 2 in 1D. The original implementation of peridynamics [Silling, 1998] was only capable of modeling materials with Poisson's ratio of one quarter which makes the method unsuitable for materials like concrete with Poisson's ratio of approximately 0.2.

Silling showed that the peridynamic method can model discontinuities of various types [Silling 1998].

2.2 Micropolar Model

In 2007, Sau proposed the micropolar peridynamic model, generalizing the original bond-based peridynamic model of Silling [Silling 1996] by adding peridynamic moments, thus allowing materials with varying Poisson's ratio to be simulated. In the original micropolar model [Gerstle et al. 2007], an infinite number of infinitesimal force-displacement relations connect infinitesimally sized material particles together. These infinitesimal force-displacement relations are called "micropolar peridynamic links" [Gerstle et al. 2007].

In the static micropolar peridynamic model,

$$\int_H \underline{f}_{ij}\left(\underline{\eta}, \underline{\xi}, \underline{\theta}\right) dV_j + \underline{b}_i = \rho \underline{u} = 0 \tag{2.6}$$

and

$$\int_H \underline{m}_{ij}\left(\underline{\eta},\underline{\xi},\underline{\theta}\right) dV_j + \underline{m}_i = \underline{I}\,\underline{\ddot{\theta}} = 0 \tag{2.7}$$

where $\underline{\theta}$ is the relative rotation, $\underline{\ddot{\theta}}$ angular acceleration and $\underline{m}_{ij}$ is the moment exerted by particle j upon particle i.

Sau found the micro elastic parameters, c and d, for the micropolar peridynamic linear elastic model [Gerstle et al 2007].

For 2D plane stress conditions

$$c = \frac{6E}{\pi\delta^3(1-\mu)}, \quad d = \frac{E(3\mu-1)}{6\pi\delta(\mu^2-1)} \tag{2.8}$$

where E is the Young's modulus of the material, μ is the Poisson's ratio, and δ is the material horizon. By this work he also expressed peridynamics microelastic constants in terms of the classical macroelastic constants.

Similarly, for 2D plane strain conditions

$$c = \frac{6E}{\pi\delta^3(1-\mu-2\mu^2)}, \; d = \frac{E(1-4\mu)}{6\pi\delta(1-\mu-2\mu^2)} \quad \text{, and} \tag{2.9}$$

for 3D conditions

$$c = \frac{6E}{\pi\delta^4(1-2\mu)}, \quad d = \frac{E(1-4\mu)}{4\pi\delta^2(1-\mu-2\mu^2)}. \tag{2.10}$$

In this model Sau found that the stiffness of the simulated material near the domain boundary is reduced. The peridynamic theory converges to the classical theory as δ is decreased.

Gerstle et al., proposed a micropolar model for concrete with seven parameters: c, d, δ, s_{tens}, s_{comp}, α_{tens} and α_{comp} [Gerstle et al. 2007]. Figure 2.2 shows the micropolar model for concrete.

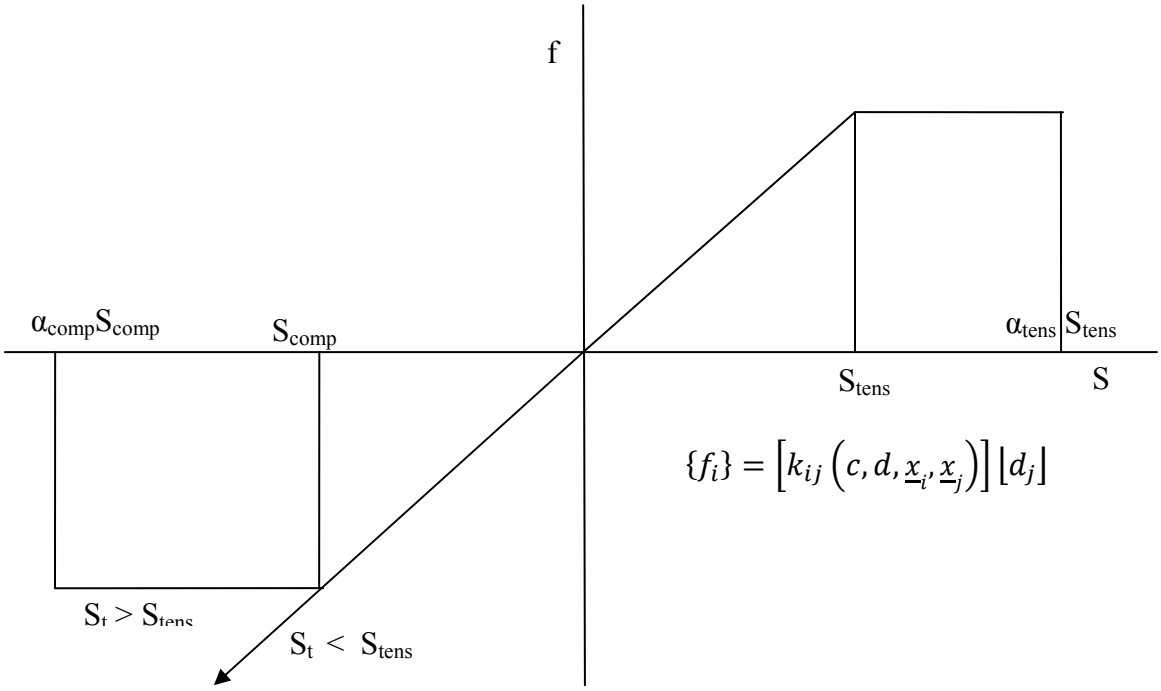

Fig. 2.2 Constitutive Behavior of a Micropolar Peridynamic Link for Concrete.

In Fig 2.2, f is the pairwise force between two particles, and S is the stretch between two particles. Stretch is the ratio of the distance between particles in the deformed configuration to the distance between the particles in the reference configuration. S_t is the maximum stretch of any link connected to the particle i.

Familiarity with the stiffness matrix is essential to understand the micropolar peridynamic model for concrete. For a bond link, a stiffness matrix [k] is a matrix relating the nodal forces {f} and nodal displacements {d}:

$$\{f\} = [k]\{d\}. \tag{2.11}$$

For a 2D model shown Fig. 2.3, the degrees of freedom are shown on Fig 2.4. The peridynamic link between two particles has an area A, length L, moment of inertia I, and the modulus of elasticity E. The force-displacement relation, assuming small deformations with respect to the length of the link is,

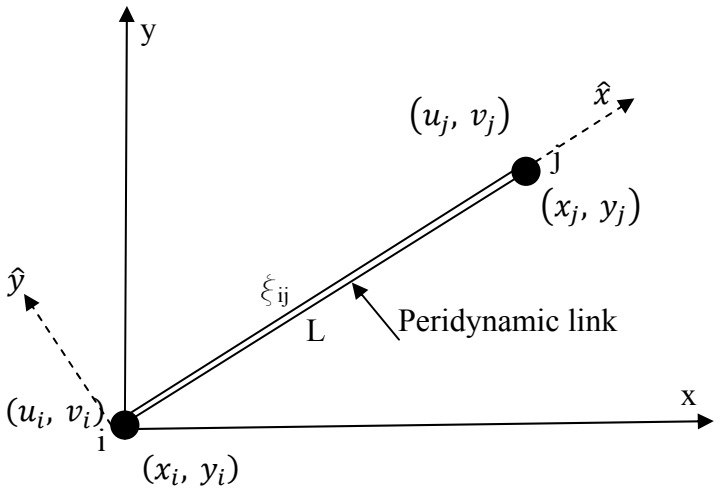

Fig 2.3 Peridynamic link for 2D

$$\begin{Bmatrix} \hat{f}_{x,i} \\ \hat{f}_{y,i} \\ \hat{m}_{z,i} \\ \hat{f}_{x,j} \\ \hat{f}_{y,j} \\ \hat{m}_{z,j} \end{Bmatrix} = \begin{bmatrix} c/L & 0 & 0 & -c/L & 0 & 0 \\ 0 & 12d/L^3 & 6d/L^2 & 0 & -12d/L^3 & 6d/L^2 \\ 0 & 6d/L^2 & 4d/L & 0 & -6d/L^2 & 2d/L \\ -c/L & 0 & 0 & c/L & 0 & 0 \\ 0 & -12d/L^3 & -6d/L^2 & 0 & 12d/L^3 & -6d/L^2 \\ 0 & 6d/L^2 & 2d/L & 0 & -6d/L^2 & 2d/L \end{bmatrix} \begin{Bmatrix} \hat{u}_i \\ \hat{v}_j \\ \hat{\theta}_{z,i} \\ \hat{u}_i \\ \hat{v}_j \\ \hat{\theta}_{z,j} \end{Bmatrix}$$

where c = EA, and d = EI.

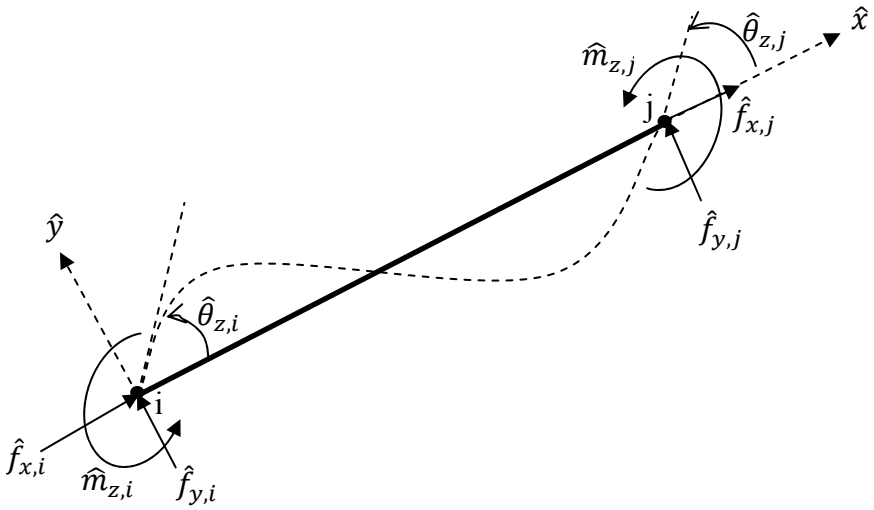

Fig 2.4 Degrees of freedoms for 2D link for linear elastic MPM

In this micropolar model, peridynamic force-displacement relations between two particles will remain linear as long as the stretch, S, is between the limits S_{comp} and S_{tens}. If the stretch, S, is more than S_{tens} then the peridynamic forces between two particles are constant up to the limit of α_{tens} S_{tens} , after which the force becomes zero so that the particles no longer interact. This model doesn't specify how moments change after S > S_{tens}.

In compression, if the stretch, S, exceeds S_{comp} there are two possibilities. First, if the maximum stretch (S_t) in any links connected to the particle 'i' is more than the linear elastic tensile limit (S_{tens}) then they follow the path designated with $S_t > S_{tens}$ in the Fig. 2.2, by which the force between particles will be constant up to the limit of S_{comp} α_{comp} after which it drops to zero. Secondly, if the maximum stretch (S_t) in any links connected to the particle "i" is less than S_{tens} then the link will not fail and it follows the path designated with $S_t < S_{tens}$. In this model, Sau just talked about the axial forces between

particles after cutoff stretch, but failed to explain the moments which is not clearly specified. In this thesis we propose a new micropolar peridynamic model for concrete and implement it within the context of lattice-based, state-based peridynamics [Rahman, 2012].

2.3 Lattice Model:

Lattice models provide a numerical model for damage and cracking of concrete. Lattice models are not new; Hrennikoff in 1941 discretized the continuum in a lattice with truss or frame elements for solving problems in elasticity [Hrennikoff 1941]. Hrennikoff showed that plane-stress problems can be modeled by discretizing a continuum with bar elements (Fig 2.5).

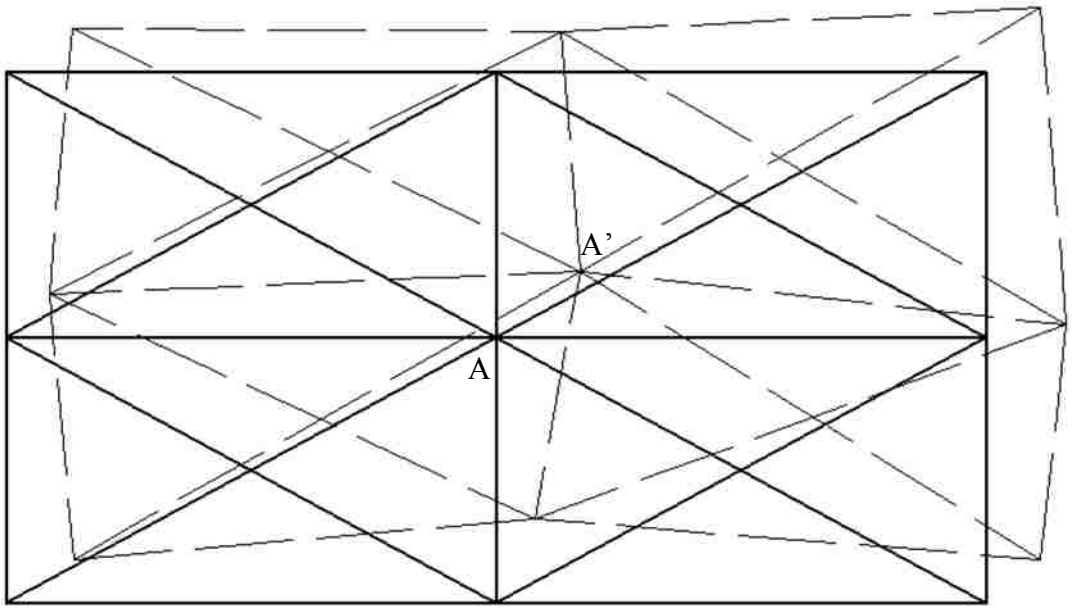

Fig. 2.5 Triangular truss (using bar elements) used by Hrennikoff. The dashed line shows the deformed mesh.

In this model the bars would need to be infinitesimally small to get the exact solution to the classical continuum elastic problem; with a finite number of elements, the

solution is only approximate. The main drawback of Hrennikoff's approach is it produces a results with a Poisson's ratio of one third which is appropriate for modeling steel structures but this approach is not appropriate for the concrete with its variable Poisson's ratio of approximately 0.2.

Hermann and his colleagues adopted the lattice model with beam elements to model fracture in concrete [Hermann et al., 1989]. Another lattice model was used for modeling fracture in concrete and sandstone laboratory-scale specimens [Schlangen et al., 1991] [Schlangen et al., 1995]. In all these models they modeled cracks by removing an element (beam or bar) as soon as its force has exceeded a certain strength criterion, which removes mass from the problem as well. Several other researchers [Burt et al. 1997] [Zubelewicz et al. 1987] [Bazant et al. 1990] have also modeled concrete fracture using the lattice model with various levels of success.

All these lattice models are discretized using beam or bar elements (with mass) to model the material specimen. On the other hand, in peridynamics the mass is concentrated at the particle level, and "elements" are used only to represent forces between particles.

2.4 Concrete Models

The lattice based peridynamic model was proposed by Asif Rahman in 2012 [Rahman, 2012], with the view of improving the micropolar peridynamic model proposed by Nicholas Sau. In this model Rahman choose the particle arrangement to be a hexagonal close-packed array. The main difference between the lattice model peridynamics and the original implementation of the peridynamics is the arrangement of particles.

Fig 2.4 and Fig 2.5 show the hexagonal close-packed particles arrangement that was chosen to model lattice-based peridynamics. Rahman obtained the following micro elastic constants.

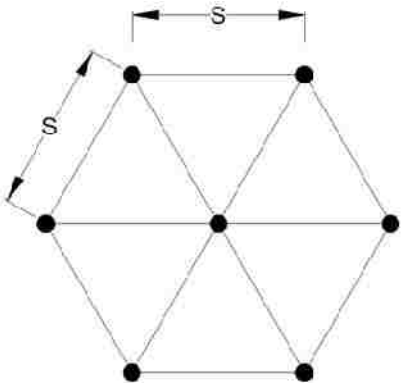

Fig 2.6 2D Lattice with six neighboring particles.

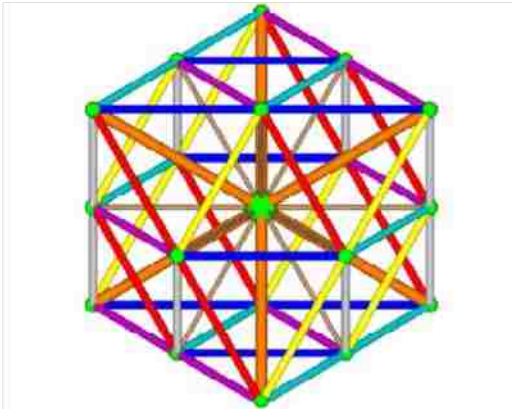

Fig 2.7 3D Lattice with 18 neighboring particles
(Source: [Rahman 2012])

For the 2D hexagonal lattice-based peridynamic model:

For plane stress problems

$$A'E' = \frac{ESt}{\sqrt{3}\,(1-\mu)} \tag{2.14}$$

$$I'E' = \frac{ES^3t(1-3\mu)}{12\sqrt{3}(1-\mu^2)}\text{, and} \tag{2.15}$$

for plane strain problems

$$A'E' = \frac{ESt}{\sqrt{3}\,(1-\mu^2)} \tag{2.16}$$

$$I'E' = \frac{ES^3t(1-4\mu)}{12\sqrt{3}(1-\mu^2)}. \tag{2.17}$$

For 3D hexagonal lattice-based peridynamic model:

$$(AE)_1 = -\frac{\sqrt{2}ES^4}{4S^2\,(\mu+1)(2\mu-1)} \tag{2.18}$$

$$(IE)_1 = -\frac{\sqrt{2}(ES^4-4E\mu S^4)}{48(\mu+1)(2\mu-1)} \tag{2.19}$$

$$(AE)_2 = -\frac{E\mu S^2}{2(\mu+1)(2\mu-1)} \tag{2.20}$$

$$(IE)_2 = 0 \tag{2.21}$$

In equations 2.18-2.21, subscript 1 is for the links with length S, and the subscript 2 is for the links with length of $\sqrt{2}$S. This lattice-based micropolar peridynamic model for concrete is shown to exhibit smaller boundary effects compared to the original implementation (bond-based) of peridynamics [Rahman, 2012]. Besides many advantages of this model such as, convergence with the solutions from theory of elasticity, Rahman's model was only developed for linear elastic problems. On the other hand, In this thesis, we implemented a new micropolar peridynamic lattice-based state-based peridynamic inelastic damage model for concrete.

There are many other models proposed by the researchers to study the behavior of concrete. But many of them are not successful to model concrete accurately. All these models can be described under two major criterions like continuum and discrete.

2.5 Dynamic Relaxation Method

This method was introduced by Sir Richard Southwell for the solution of partial differential equations using finite difference approximations. In this thesis we use this

dynamic relaxation method to damp the model to achieve the steady state solution. This method does not require matrix manipulations for the solution of the system of non-linear equilibrium equations [Lewis, 2003]. The system oscillates about the equilibrium position and comes to the rest with influence of 'damping'. We employed viscous damping method in our solution.

Dynamic relaxation method with viscous damping

Fig.2.7(a) and Fig.2.7(b) show the undamped and the damped oscillations of a simple pendulum under external force P. We want our structures to be critically damped. The equation of motion for a discretized system of particles is given by the following equation,

$$P = [\sum K\delta] + M\ddot{\delta} + C\dot{\delta} \qquad (2.15)$$

where, P is the vector of external loads, $[\sum K\delta]$ is the vector of internal forces with K respresenting the stiffness and δ is the vector of displacements, C is the damping matrix , $\ddot{\delta}$ is the vector of nodal accelerations and $\dot{\delta}$ is the vector of nodal velocity.

Critical viscous damping coefficient (C)

The static or steady state solution cannot be achieved without viscous damping coefficient. For undamped oscillations shown in Fig.2.7 (a) the structure will oscillate for infinite time. Fig.2.7 (b) shows the solution for the case of damped oscillations. If the damping coefficient is less than critical damping factor then the solution will overshoot static equilibrium and the system is said to be under-damped.

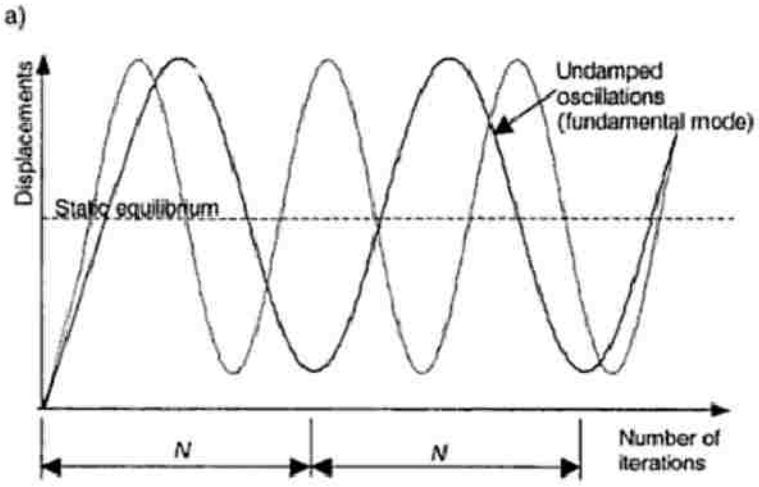

Fig 2.7 (a) Undamped oscillations

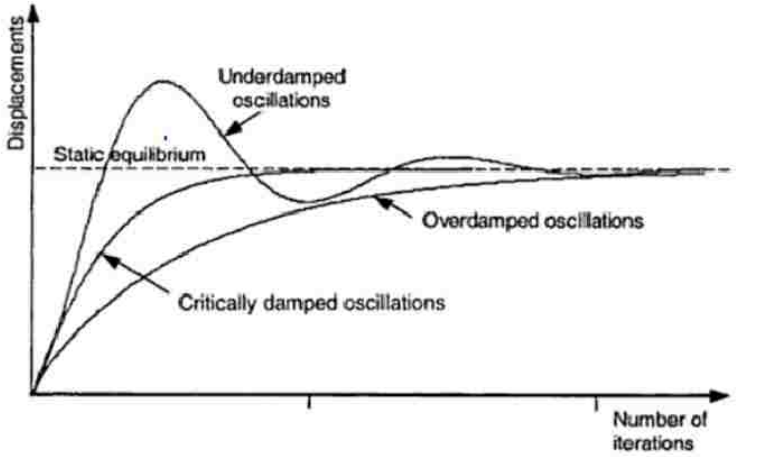

Fig 2.7 (b) Damped oscillations of displacement in dynamic relaxation method (Adopted from Lewis 2003)

The convergence to the static or steady solution is quicker in critically damped conditions. For this purpose a critical damping factor was chosen in order to achieve the solution in pdQ as fast as possible, this reduces the computation efforts and time. More details concerning critical damping and dynamic effects are discussed in Chapter 5 (Example).

Chapter 3. Peridynamic Model for Concrete.

In this chapter we present a new, lattice-based, micropolar peridynamic model for concrete, with the capability to model damage in both tension and compression. This model is similar to the very old strut-and-tie model for concrete [Yun, 1996]. The micropolar peridynamic model was originally proposed by Gerstle and his students [Gerstle at al., 2003] to overcome a drawback of the original peridynamics bond-based model, namely, that it models only materials with Poisson's ratio of one-quarter ($^1/_4$).

The new model is applicable to 1D, 2D, and 3D problems. In this thesis, for brevity, we restrict our attention to 2D models. We start by assuming a 2D hexagonal lattice of particles in the reference configuration, as shown in Fig.3.1.

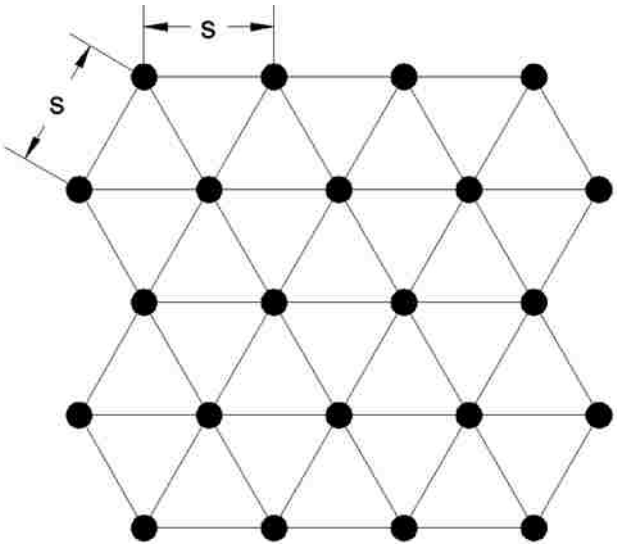

Fig. 3.1 – 2D hexagonal lattice of particles.

In 2D, the material horizon, δ, is chosen so that each particle interacts only with its six nearest neighbors, all at a distance 's' away from it. We refer to each of these force interactions as a "link". Referring to Fig. 3.2, the force-displacement relationship between neighboring particles includes two damage parameters, ω_t and ω_c. Both the parameters vary between 0, representing no damage, and 1, representing complete

damage, and because concrete is assumed not to "heal", both damage parameters are assumed never to decrease with time.

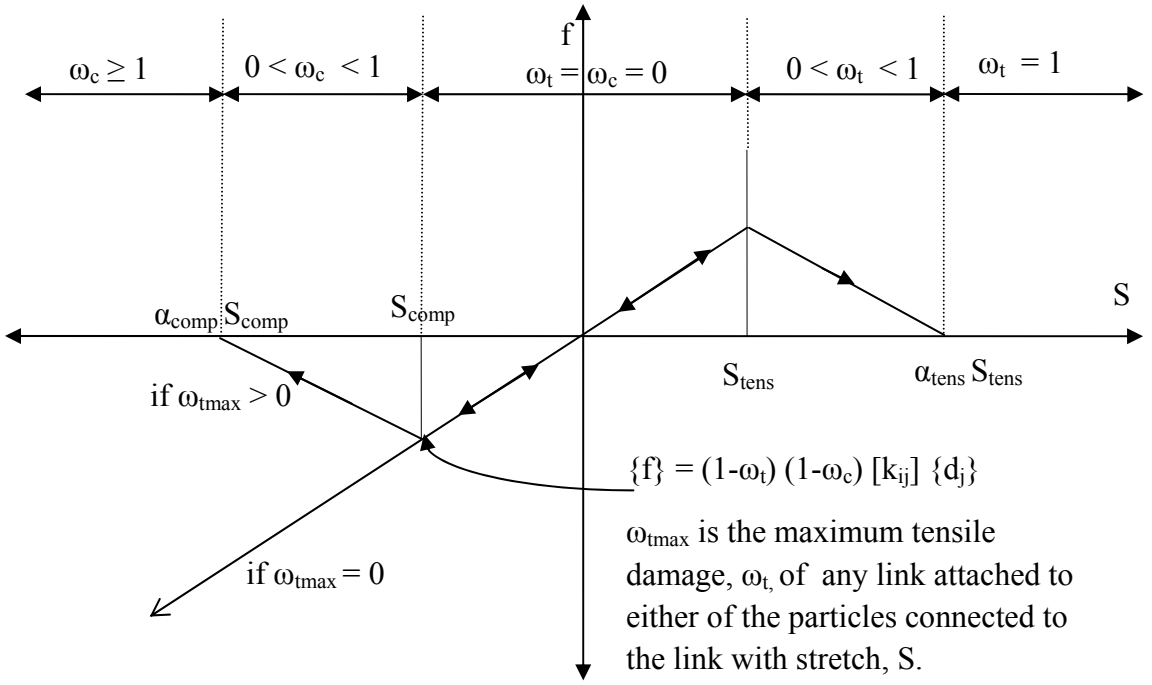

Fig. 3.2 Modified micropolar model for concrete

The pairwise force vector, $\{f_{ij}\}$, acting between the particles i and j is represented by

$$\{f_i\} = (1-\omega_t)(1-\omega_c)[k_{ij}]\{d_j\} \quad (3.1)$$

where ω_t is the tensile damage parameter and ω_c is the compressive damage parameter associated with the link between particle i and j.

A peridynamic link between the particles i and j for the micropolar model is assumed to have the same forces as a frame element as shown in Fig. 3.3.

Referring to Fig. 3.3, the linear force-displacement relationship between two neighboring particles, $\{f\} = [k]\{d\}$, is developed assuming the 2D linear elastic hexagonal lattice-based peridynamic model [Rahman, 2012].

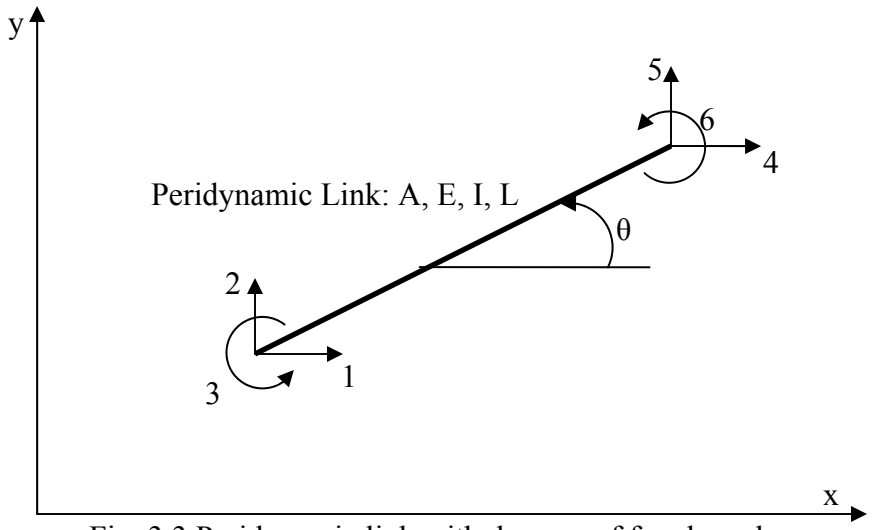

Fig. 3.3 Peridynamic link with degrees of freedom shown.

Rahman represented the axial (A'E') and the flexural rigidity (I'E') of the latticed-based 2D peridynamic link for the plain stress condition as

$$A'E' = \frac{2E*d_{vol}}{3(1-\mu)*S} \quad \text{and} \quad I'E' = \frac{E*d_{vol}*(1-3\mu)*S}{18*(1-\mu^2)}. \tag{3.2}$$

From the recent work for the lattice-based peridynamic model for plain stress conditions [Rahman, 2012], Equation 3.1 can be rewritten in terms of peridynamic parameters as.

$$\begin{Bmatrix} f_1 \\ f_2 \\ m_3 \\ f_4 \\ f_5 \\ m_6 \end{Bmatrix} = (1-\omega_c)(1-\omega_t) * [\mathrm{k}] * \begin{Bmatrix} d_1 \\ d_2 \\ d_3 \\ \theta_4 \\ d_5 \\ \theta_6 \end{Bmatrix} \tag{3.3}$$

where [k] is the stiffness matrix, given by

$$\mathrm{k} = \begin{bmatrix} (C_1c^2 + C_2s^2) & (C_1 - C_2)cs & -C_3s & -(C_1c^2 + C_2s^2) & -(C_1 - C_2)cs & -C_3s \\ (C_1 - C_2)cs & (C_1s^2 + C_2c^2) & C_3c & -(C_1 - C_2)cs & -(C_1s^2 + C_2c^2) & C_3c \\ -C_3s & C_3s & C_4 & C_3s & -C_3s & C_5 \\ -(C_1c^2 + C_2s^2) & -(C_1 - C_2)cs & -C_3s & (C_1c^2 + C_2s^2) & (C_1 - C_2)cs & C_3s \\ -(C_1 - C_2)cs & -(C_1s^2 + C_2c^2) & -C_3c & (C_1 - C_2)cs & (C_1s^2 + C_2c^2) & -C_3c \\ -C_3s & C_3s & C_5 & -C_3s & -C_3s & C_4 \end{bmatrix},$$

where c = cos(θ), s = sin(θ), $C_1 = \frac{2*E*d_{vol}}{3*s*L*(1-\mu)}$, $C_2 = \frac{2}{3*L^3}\frac{E*d_{vol}*(1-3\mu)}{(1-\mu^2)} * s$, $C_3 = \frac{1}{3*L^2}\frac{E*d_{vol}*(1-3\mu)}{(1-\mu^2)} * s$, $C_4 = \frac{2}{9*L}\frac{E*d_{vol}*(1-3\mu)}{(1-\mu^2)} * s$, $C_5 = \frac{1}{9*L}\frac{E*d_{vol}*(1-3\mu)}{(1-\mu^2)} * s$, in which E is the Young's modulus of the material, L is the length of the link, d_{vol} is the volume of the particle, μ is Poisson's ratio, and s is the spacing of the particles. In the Equation 3.3, small deformations theory is not assumed and the stiffness of the link is calculated at every time step including large rotation of the link.

In above equation, spacing of the link, s, and the length of the link, L, is represented by the current distance between the two particles.

The damage factor (ω_t or ω_c) is zero as long as the stretch in the link between two particles remains elastic, after which ω_t is the function of the maximum stretch, S, of the link. If we observe the forces being calculated between the particles for a peridynamic link, they are dependent on axial and flexural rigidities of the link. In our model, the damage factors depend only on stretch, S. This may be an over-simplification, as it would appear that shear and bending damage may depend upon shear and bending deformations, in addition to the stretch of the link. In future work, a more precise model will perhaps be developed accounting for damage due to shear and flexural deformations.

The tensile damage factor, ω_t, is defined as follows:

for $S \leq S_{tens}$,

$$\omega_t = \max\{0, \omega_{t(prev)}\},$$

for $S_{tens} \leq S$,

$$\omega_t = \min\left\{\max\left(\frac{(S - S_{tens})}{(\alpha_{tens}S_{tens} - S_{tens})}, \omega_{t(prev)}\right), 1\right\}$$

where, $\omega_{t(prev)}$ is the maximum tensile damage factor of the link at any previous time.

On the other hand, we assume that damage in a link in compression can occur only if there is tensile damage in any of the links connected to either of the particles associated with the link. This is because a compression strut of concrete is strong in compression, but if any other link connected to the either of the particles has a tensile damage then the strut loses lateral stability. If any of the other link connected to a particle associated with the link has tensile damage ($\omega_t > 0$), then the link with sufficient compressive stretch is assumed to experience compressive damage and

for $S_{comp} \leq S$,

$$\omega_c = \max\{0, \omega_{c(prev)}\}, \text{ while}$$

for $S \leq S_{comp}$,

$$\omega_c = \min\left\{\max\left(\frac{(S - S_{comp})}{(\alpha_{comp} S_{comp} - S_{comp})}, \omega_{c(prev)}\right), 1\right\}.$$

We assume that the peridynamic link cannot fail in compression, i.e it cannot have any damage ($\omega_c = 0$) if all the other links connected to either of the particles to which it is connected have stretches within elastic limits.

In this chapter a new micropolar peridynamic damage model for concrete has been proposed. Calibration of the seven parameters (s, α_c, S_c, α_t, S_t, E, μ) for this new micropolar, state-based peridynamic damage model for cementitious material are described in the Chapter 4.

Chapter 4. Calibration of Peridynamic Parameters

In this chapter the peridynamic material parameters for the concrete model are calibrated. The results from this calibrated model are compared with the predictions of the American Concrete Institute (ACI) code. Various simulations are modeled to obtain material parameters, by trial and error. The basic material parameters for the micropolar, lattice-based, state-based peridynamic model are spacing, s, Young's modulus, E, Poisson's ratio, μ, critical tensile stretch S_{tens}, critical compression stretch S_{comp}, constants α_t and α_c. Damage factors evolve in the simulations based on these calibrated parameters. The parameter s is chosen either based on upon aggreagate size or upon computational considerations. E and μ are used to obtaion the microelastic problem parameters C_1, C_2, C_3, C_4, C_5, and C_6,

4.1 Concrete in Tension:

Concrete is weak in tension when compared to its compressive strength. The tensile strength of concrete is approximately 8% to 15% of its compressive strength. For uniaxial tensile loading, cracks will propagate in a direction perpendicular to the applied loads.

To calibrate concrete in tension, various models have been simulated, an average value of critical stretch, S_{tens}, is found. For all the concrete plate models, an axial load is applied to the three layers of particles on both the top and bottom of the plate as shown in Fig. 4.1. An example of a concrete plate with dimensions of 15" x 45" x 1" is shown in Fig. 4.1.

With reference to the Fig. 4.1, the particles are displayed with a color code. A green color node represents a particle which is free to move in the X and Y directions, while the blue color nodes represent a particle that is loaded in the Y-direction (axial loading). Equal and opposite vertical loads are applied to the particles that are in upper the and lower three layers.

A particle is chosen to monitor the deformations as a function of time. The complete data of this particle is written to a separate file and the required time history graph is plotted. By observing this time history graph, one can easily identify whether the model has damped to the steady state solution, or failed.

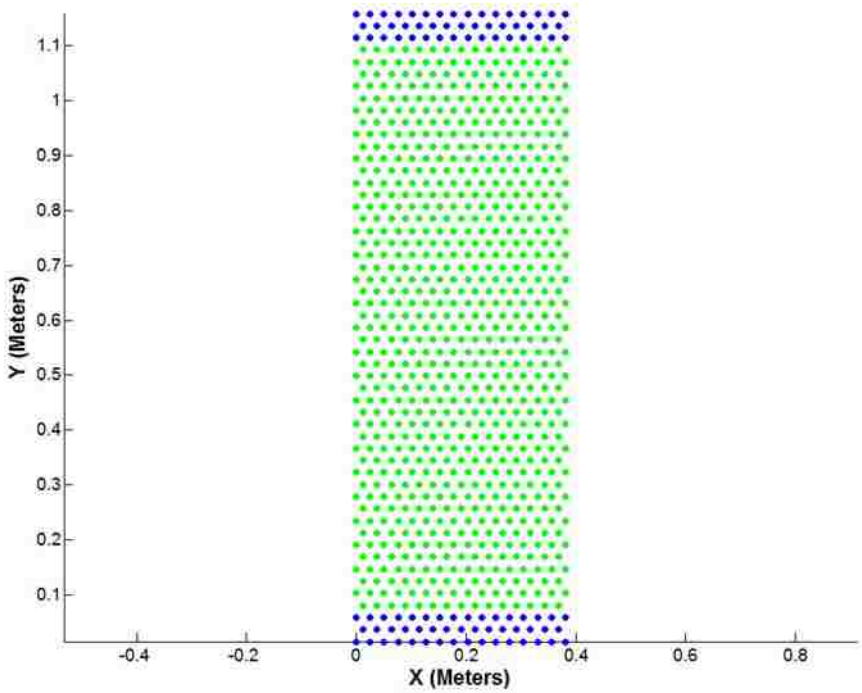

Fig. 4.1 Concrete plate 15" x 45" x 1" modeled for calibration.

Fig 4.2 shows a time history plot (displacement versus time) of the extreme upper right particle. It is clear from this graph that after 1,500 time steps there is no further

change in the position of the particle. This confirms that a steady state solution has been achieved. Fig. 4.3 shows the deformed shape of concrete plate subjected to axial tension after the steady state solution has been achieved. The deformations have been magnified by a factor of 5,000. This simulated model did not fail in tension. In subsequent trial the load is increased to find the failure load of the specimen. Various simulations are modeled by changing the load and the critical stretch, S_{tens}. The critical stretch, S_{tens}, of the model for concrete is assumed to have been determined when the failure load from pdQ is approximately equal to the tensile strength, f'_t, of the concrete.

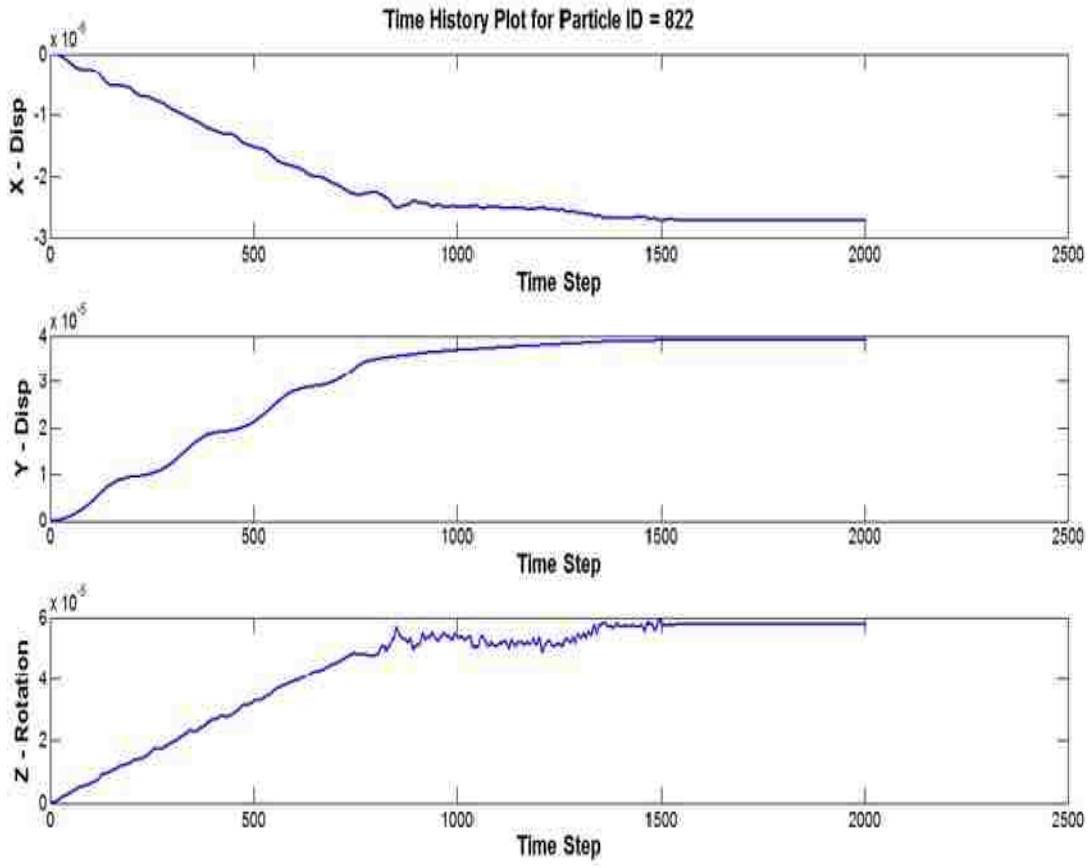

Fig. 4.2 Time history plot of the concrete plate loaded in tension.

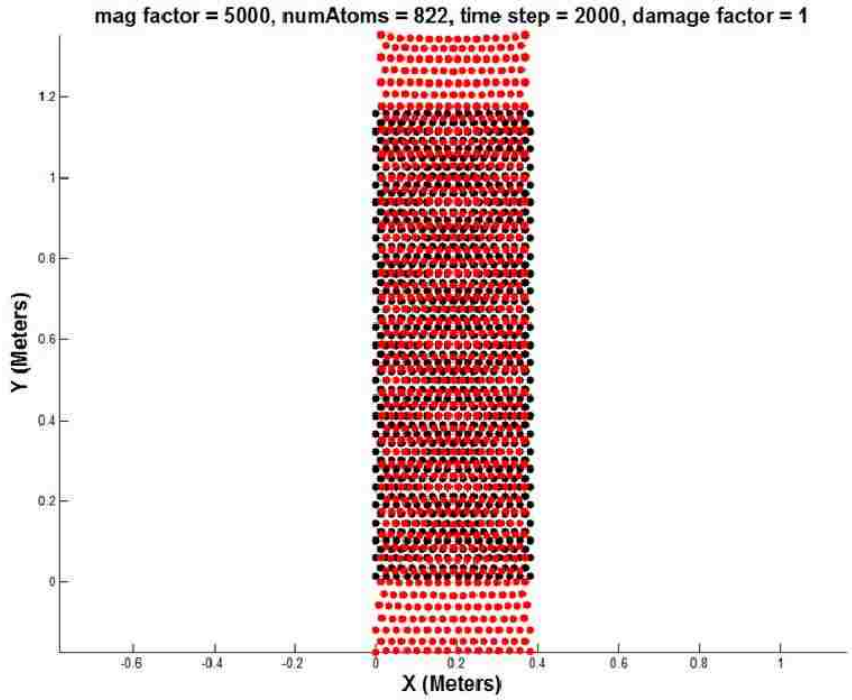

Fig. 4.3 Deformed shape of concrete plate in tension

Fig. 4.4 shows the deformed shape of the concrete plate after failure. To compare the deformed shape of the concrete plate, a reference configuration of the concrete plate is plotted to the left. The damaged links are plotted in a green color. A time history plot is shown in Fig. 4.5 that shows that the monitored particle started accelerating after timestep 1,500. The load ramped gradually upto the twice the fundamental time period of the concrete plate. Total time of simulation is three times the fundamental time period. It appears that the deformations are zero up to 1,500 time step (5.0E-3 sec), but actually the deformations are very small compared to the deformations after 1,500 time step (5.0E-3 sec), where the particle started accelerating with large deformations.

This concrete plate model failed in tension when the cracks initiated between the loaded and unloaded layers of particles. As the tensile load is being applied to both top

and bottom layer with equal and opposite magnitude, the fracture of the plate is expected to appear near the top and bottom loaded layers and the crack propagates along the horizontal direction.

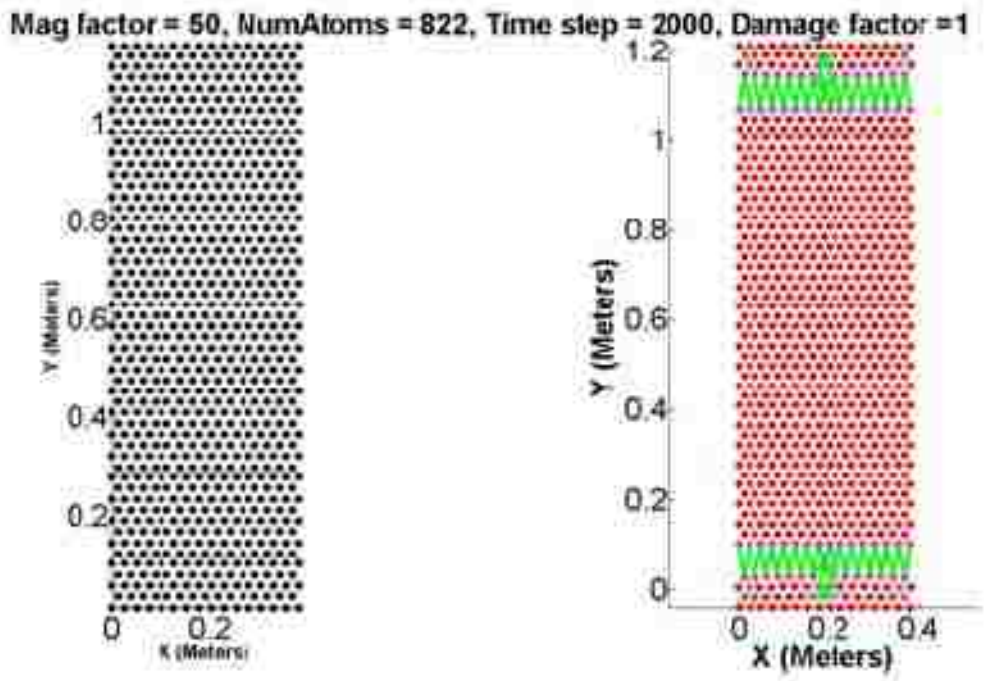

Fig. 4.4 Deformed shape of concrete plate with tension cracks.

This is the similar cracking behavior predicted by other researchers [Huang, 2011]. We can see that with the magnification factor is set to 50, we are able to see large deformations with the initiation of cracks. Time history plot shows that the deformation of the particle is increasing as the time of simulation increases. This implies that no steady-state solution exits, and the plate has failed.

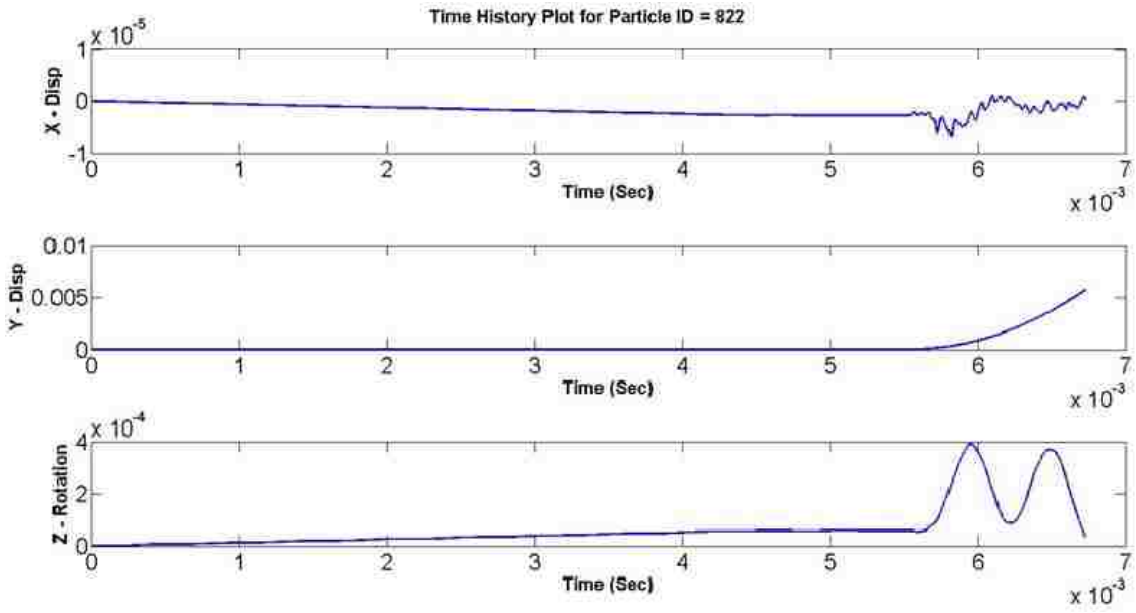

Fig. 4.5 Time-history plot of concrete plate loaded in tension.

The direct tensile strength of the concrete is calculated from the report "cracking of concrete members in direct tension", ACI Committee 224. With reference to ACI 209R, the following equation estimates the tensile strength, f'_t, of the concrete for direct tension as the function of uniaxial compressive strength, f'_c [ACI, 1997].

$$f'_t = g_t [w_c f'_c]^{1/2} \qquad (4.1)$$

where w_c is the unit weight of concrete (lb/ft^3), f'_c is the compressive strength of concrete (lb/ft^2), and $g_t = 0.33$. For normal-weight concrete with f'c = 4,000psi,

$f'_t = 0.33 * (145*4000)^{1/2} = 251$ psi.

Load P_t = area x f'_t = 15 in * 1 in * 251 psi = 3,765 lbs

=16,746 Newtons

Load per each of the 47 loaded particles =356 N/Particle

The material property, S_{tens}, is adjusted to fail the model at the same load that was calculated from the ACI codes.

Load per each 47 loaded particles from pdQ = 360 N/Particle.

If f'_t is the strength of the concrete, then since

$$E\ \varepsilon'_t = f'_t \tag{4.2}$$

Where ε is the tensile strain of the concrete, E is the Young's modulus of the concrete.

From Equation 4.2, using, $E = 57000\sqrt{f'_c}$, $\varepsilon = S_{tens} = \frac{f'_t}{E} = \frac{251\ psi}{3604{,}000\ psi} = 0.0000696$

The average critical tensile stretch, S_{tens}, was found to be 0.00006034. The ratio of the critical stretch, S_{tens} to the limiting strain in tension from ACI is 0.87. We can express the relationship between tensile critical stretch, , S_{tens}, and the limiting tensile strain from ACI code as,

$$S_{tens} = \frac{0.00006034}{0.00006960}\ \frac{f'_t}{E} = 0.87\ \frac{f'_t}{E} \tag{4.3}$$

Table 4.1 summarizes the various models that we considered for calibrating the concrete in tension.

Table 4.1 Concrete Plates Considered for Tension Models

	Number of particles loaded	Load at failure (N/Particle)		Difference: (pdQ-Exact)/Exact
		pdQ	ACI	
5 x 15	17	365	327	11.62
15 x 45	47	355	360	-1.39
20 x 60	62	360	360	0.00
30 x 90	92	358	363	-1.38
40 x 120	122	355	365	-2.74
60 x 180	182	367	355	3.38
80 x 240	242	355	368	-3.53

4.2 Concrete in Uniaxial Compression

The uniaxial compressive strength, f'_c, of concrete is the standard property the concrete that engineers use in designing concrete structures. Compressive strength of concrete is found from laboratory testing using the universal testing machine. Fig. 4.6 shows a concrete specimen that has failed in compression. The concrete plate shown in Fig. 4.1 is now axially loaded in compression and a similar study is conducted to find the critical stretch in compression. The concrete is weak in tension, thus a concrete specimen that is loaded in compression first fails transversely in tension due to the Poisson's effect.

Fig. 4.6 Concrete specimen failed in compression test.
[NRMCA, 2003]

Fig 4.7 is a time history plot for the concrete plate axially loaded in compression. This time history plot also shows the convergence of the solution to the steady state solution. The critical damping factor was chosen so as to damp the model monotonically to a steady state solution. Fig. 4.8 shows the elastic deformed shape of the axially loaded concrete plate in compression. Black particles represent the reference position and red particles represent deformed position. Deformations are magnified by a factor of 2,000.

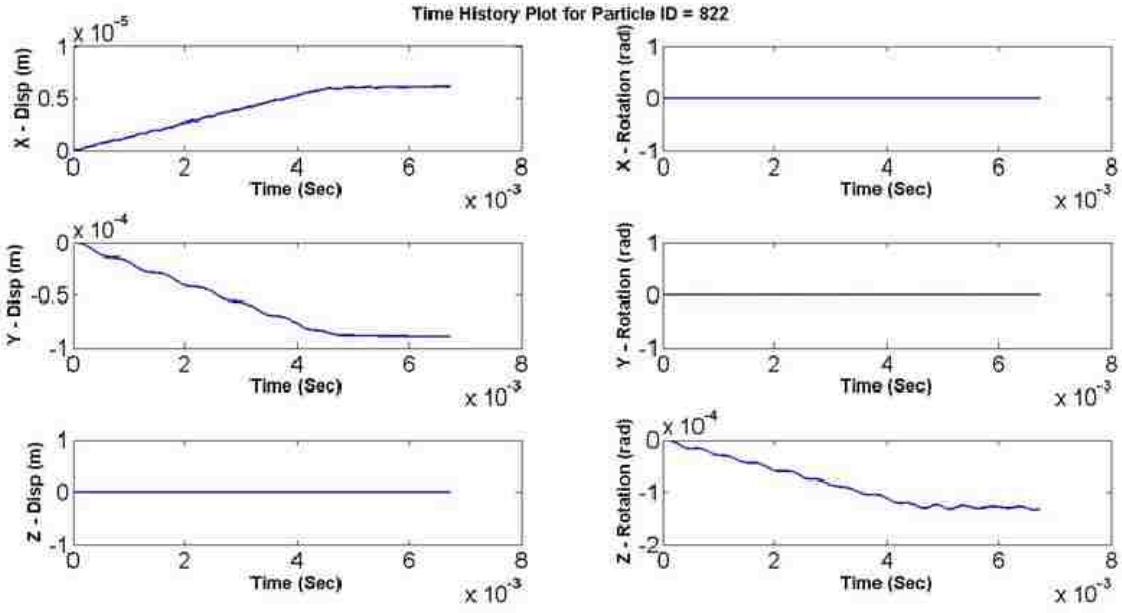

Fig. 4.7 Time history plot of concrete plate loaded in compression

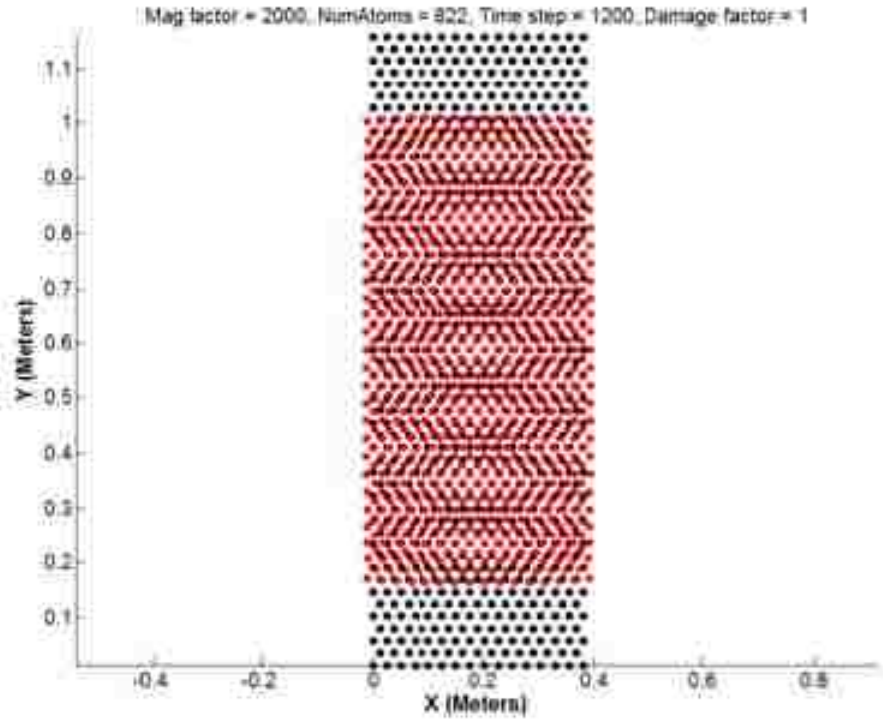

Fig. 4.8 Deformed shape of concrete plate in compression.

Fig. 4.9 and Fig. 4.10 refer to a model that failed in compression. The time history plot shows that the deformation of the particle is increasing as the time of simulation increases. This implies that particles are not experiencing any bond between neighboring particles. They are free to move with constant acceleration.

Tensile damage shown with green lines are shown in Fig 4.10, which is expected from classical mechanics. Crushing of the particles is represented by the breaking of compressive links which is shown by blue lines.

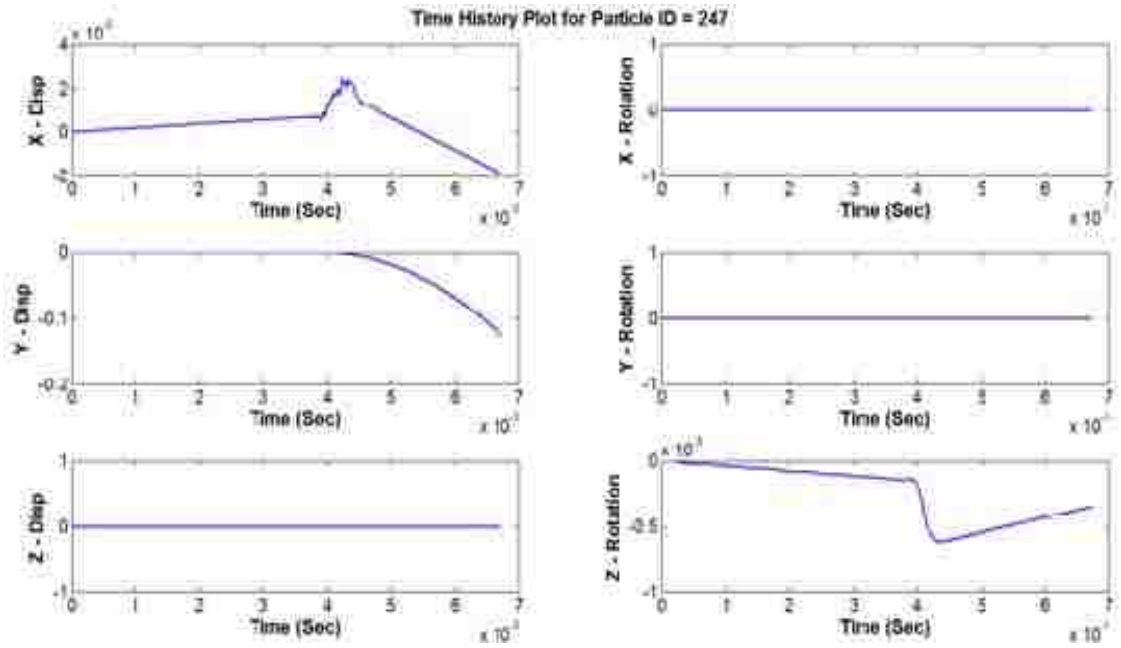

Fig. 4.9 Time history plot of concrete plate loaded in compression

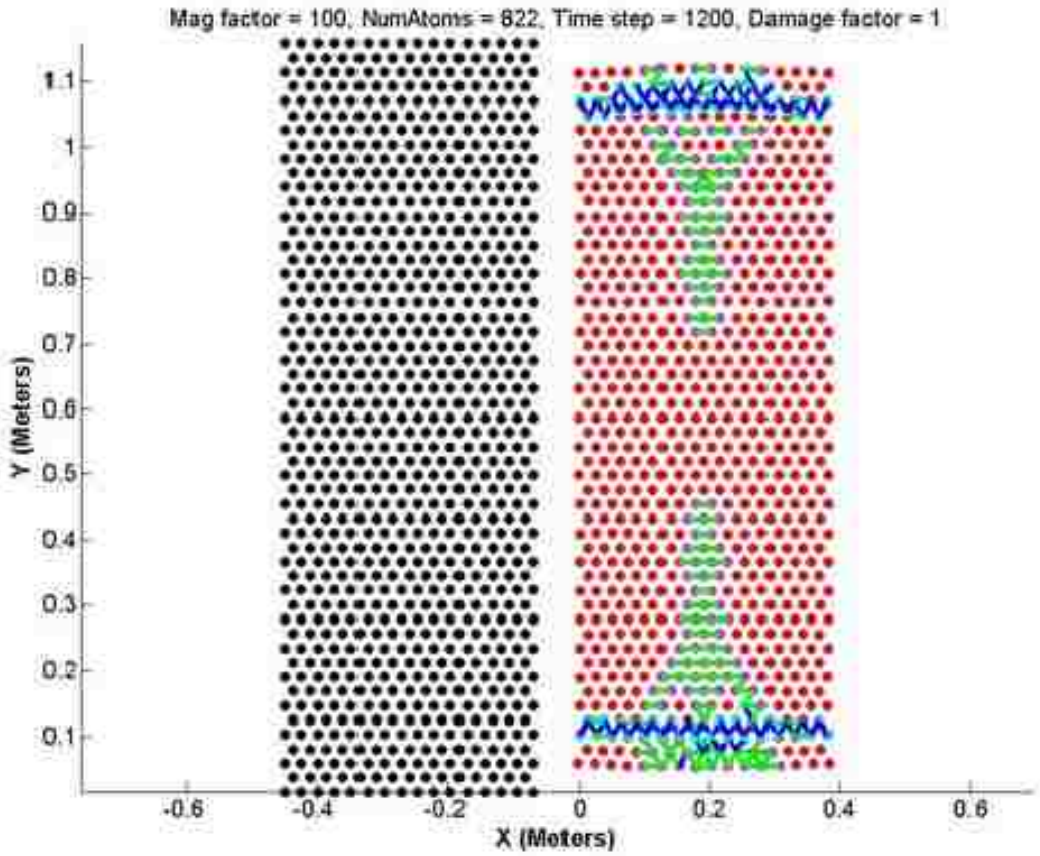

Fig. 4.10 Deformed shape of concrete plate failed in compression.

In this study the strength of concrete in compression is taken as ten times the strength of concrete in tension (f'_t). Though the concrete strength is 4,000 psi, concrete exhibits some softening behavior earlier than f'c. The compressive strength of concrete used for calibration in compression is f'c = 2,510 psi.

If f'_c is the strength of the concrete, then since

$$E\,\varepsilon'_c = f'_c \tag{4.4}$$

Where ε is the compressive strain of the concrete, E is the Young's modulus of the concrete.

From Equation 4.4, using, $E = 57000\sqrt{f_c'}$,

$$\varepsilon = S_{comp} = \frac{f_c'}{E} = \frac{2510\ psi}{3605{,}000\ psi} = 0.000696 \quad (4.5)$$

The average critical compressive stretch, S_{comp}, was found to be 0.00061875. The ratio of the compressive critical stretch, S_{comp} to the limiting strain in compression is 0.88. We can express the relationship between compressive critical stretch, , S_{comp}, and the limiting tensile strain from ACI code as,

$$S_{comp} = \frac{0.00061875}{0.000696}\frac{f_c'}{E} = 0.88\ \frac{f_c'}{E} \quad (4.6)$$

An example calculations for the concrete plate shown in Fig. 4.1 loaded in compression is shown below;

Allowable stress (f'c) = 2,510 psi

Loaded area = 15" x 1" = 15 Sq. In

Load at failure = 2,510 x 15 x 1 = 37,650 lbs

= 167,467.2 N

Load per each of the loaded 47 particles

from Equation 4.5 = 3563.0 N / Particle

Load per each of the loaded 47 particles

from pdQ = 3600.0 N / Particle

Critical compressive stretch S_c = 0.00061875

Table 4.2 summarizes the various models that are considered for calibrating the concrete model in compression.

Table 4.2 Concrete Plates Considered for Compression Models

Dimensions	Number of Loaded Particles	Load at failure (N/Particle)		Difference:
		pdQ	ACI load at failure	$\frac{pdQ - Exact}{Exact} \times 100$
15 x 45	47	3600	3563	1.04
30 x 90	92	3640	3583	1.57
40 x 120	122	3660	3738	-2.08

4.2 Concrete in Confined Compression

In this section the behavior of the concrete model under confined compression is investigated. The strength of the concrete plate is expected to be unbounded when loaded in hydrostatic compression.

The concrete plate shown in Fig. 4.8 is loaded axially in compression with the confined boundary in the lateral direction. We allow the plate to compress in the longitudinal or the loaded direction. The boundary particles are restricted from moving horizontally. The Top three layers of particles are loaded.

From the concrete model defined in Chapter 3 for lattice based state-based, micropolar peridynamics, we expect that the concrete should not fail in compression due to the restricted stretch in links in the lateral direction (tension). For concrete to fail in compression, there must be at least one tensile link that exceeds the elastic limit. Fig 4.12

confirms that the model defined for concrete represents the features of the concrete. The applied load for this model exceeds more than 16 times the strength of the concrete in tension, and the model is in linear elastic without any sign of damage.

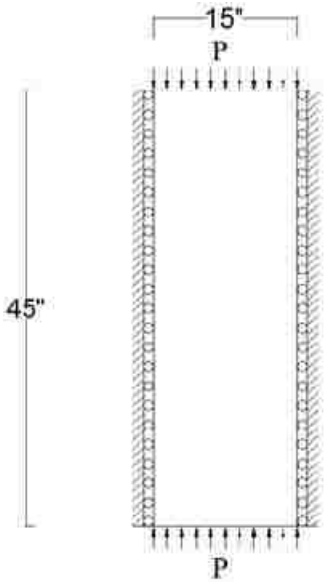

Fig. 4.11 Concrete plate 15" x 46" with confined boundaries

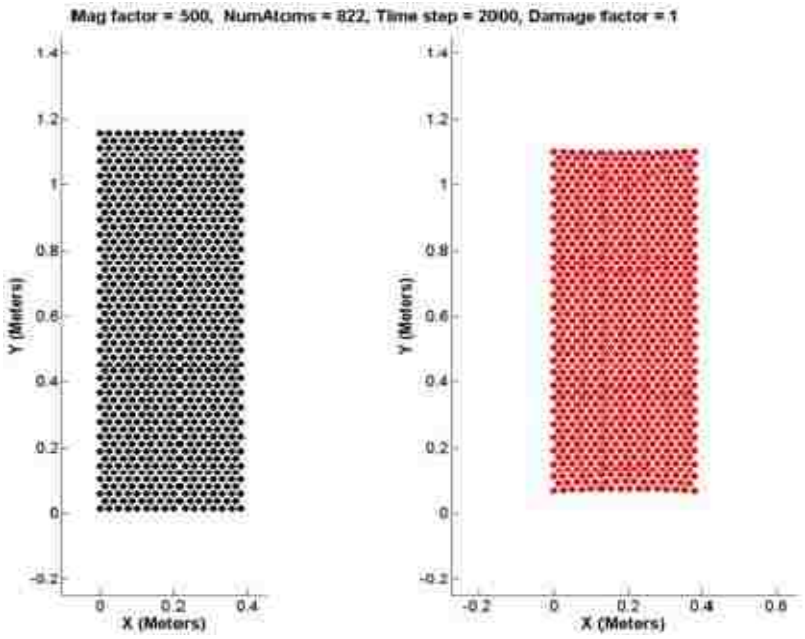

Fig. 4.12 Deformed concrete plate 15" x 46" with confined boundaries

We observe from the Fig. 4.12 that the concrete deformed significantly in the longitudinal direction. But the concrete doesn't experience any damage. This confirms the capability of modeling features of the concrete in confined compressions.

The summary of the calibrated lattice-based, state-based, peridynamic damage model for concrete presented in this chapter is,

$$S_{tens} = 0.87 \frac{f_t'}{E}$$

$$S_{comp} = 0.88 \frac{f_c'}{E}$$

$$\alpha_{tens} = 2$$

$$\alpha_{comp} = 5.$$

In this study we didn't calibrate the parameter α for both compression and in tension. As the peridynamic material parameters for the concrete model has been defined in this chapter, it is necessary to check and verify the results. In the next Chapter 5, we simulate example problems with known behavior and verify the results from concrete model.

Chapter 5. Examples

In this chapter example problems are presented to demonstrate the applicability of the concrete model proposed in Chapter 3. Various bench mark problems with known behaviors are modeled using pdQ and compared with the results predicted by the ACI code.

As expected, many problems simulated using pdQ show variability of results with respect to rate of loading. Fig. 5.1 shows the deformed shape of the concrete plate shown in Fig. 4.1 with load increased gradually up to the fundamental time period of the structure (T) after which the load is held constant. The total time of simulation (3T) for this problem is three times the fundamental time period. Fig. 5.2 shows the deformed shape of the same concrete plate but with a different rate of loading.

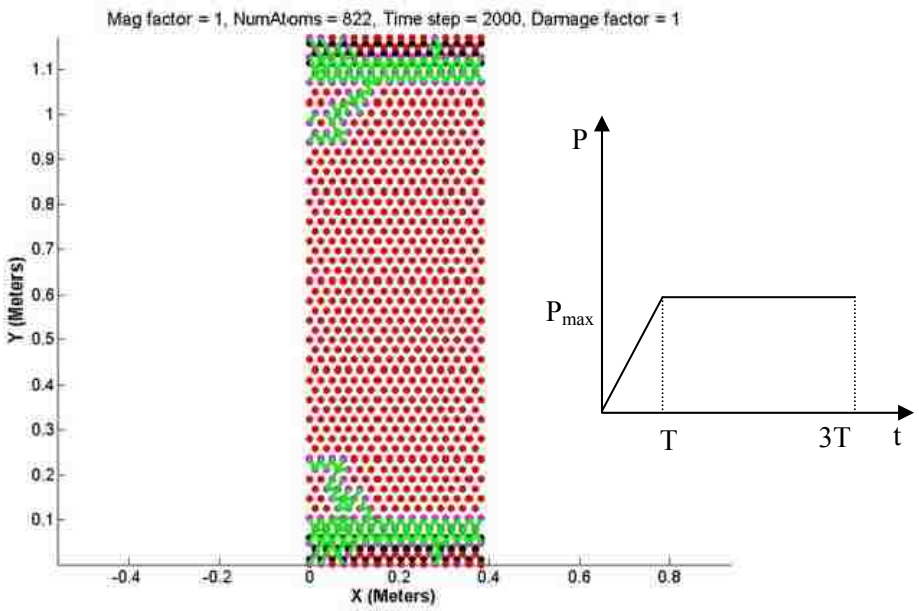

Fig 5.1 Concrete Plate under uniaxial tension with rampforce for time T

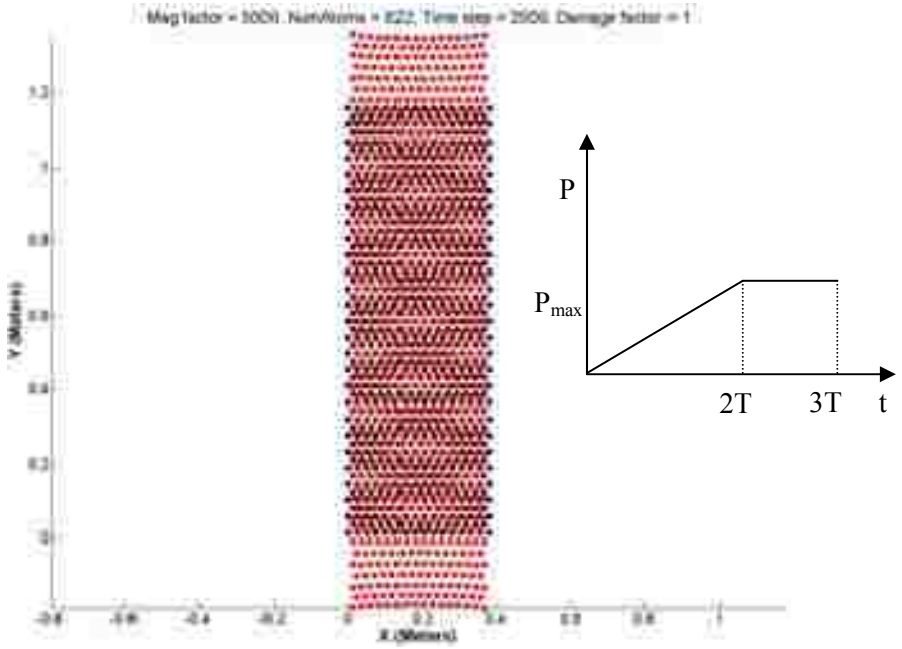

Fig 5.2 Concrete plate under uniaxial tension with rampforce for time 2.0T

Load for the model in Fig 5.2 increased linearly from zero to two times the fundamental period of the structure, after which the load is held constant. The total time of simulation (3T) for the model is again three times the fundamental time period of the structure. This shows the dependence of the results up on the rate of loading. The model with the higher rate of loading failed earlier than the model with the lower rate of loading.

All the examples in this thesis are simulated for a time of three times the fundamental time period of the structure. A standard rate of loading is employed to compare models and to calibrate the material parameters. The load is increased linearly from zero up to the twice the fundamental period of the structure.

Dynamic Factor

We employed viscous damping in our solutions as explained in Chapter 2.

5.1 Unreinforced Simply Supported Beams

Fig. 5.3 shows a simply supported beam of dimensions 30” x 6” x 11”. The particle spacing is one quarter of an inch. The left support is a pin, and the right support is a roller. A uniformly distributed load is applied to the top of the beam as shown in Fig.5.3.

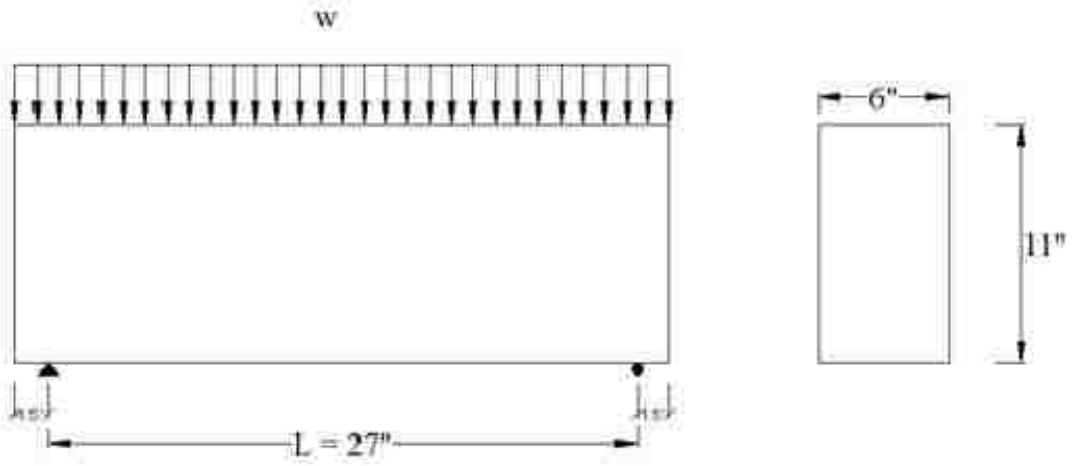

Fig. 5.3 Description of a simply supported beam

This cantilever beam has strength of 1,200 lbs/in. PdQ models this cantilever beam as stable until a load of 1,200 lbs/in is applied. If the load is further increased, then a flexural crack emerges from the bottom of the mid span, as expected.

A personal computer with Intel Core 2 Duo T6600 @ 2.20 GHZ 2.20 GHz processors and 4 GB ram was used to run the simulation. With this computer, it takes 33 minutes to complete the simulation. If the particle spacing were increased to one inch then the total number of particle interactions would be reduced. But with the coarser particle spacing the resolution of the cracks is not as clear.

From classical mechanics we know that, before cracking the maximum flexural stress occurs at mid span, so it is expected that the crack will initiate from the bottom mid span of the beam.

Using L = 27", f'_t = 251 psi, c = 5.5", and I = $\frac{6 \times 11^3}{12}$ = 665.5 in^4,

$$M_{max} = \frac{w L^2}{8} = \frac{f_t I}{C} = 30{,}371 \text{ lb-in}$$

The load at which beam fails is w = 270 lb/in.

A load of 300 lbs/in is applied on the beam shown Fig. 5.3. Fig. 5.4 shows the deformed configuration of the beam with damage. A flexural crack emerges from mid span where the bending moment is maximum for a simply supported beam. Crack propagation is not symmetrical to the span; this may be due to the unsymmetrical behavior of the supports (hinge and roller). This model also shows the damage over the supports, which is expected due to the stress concentration.

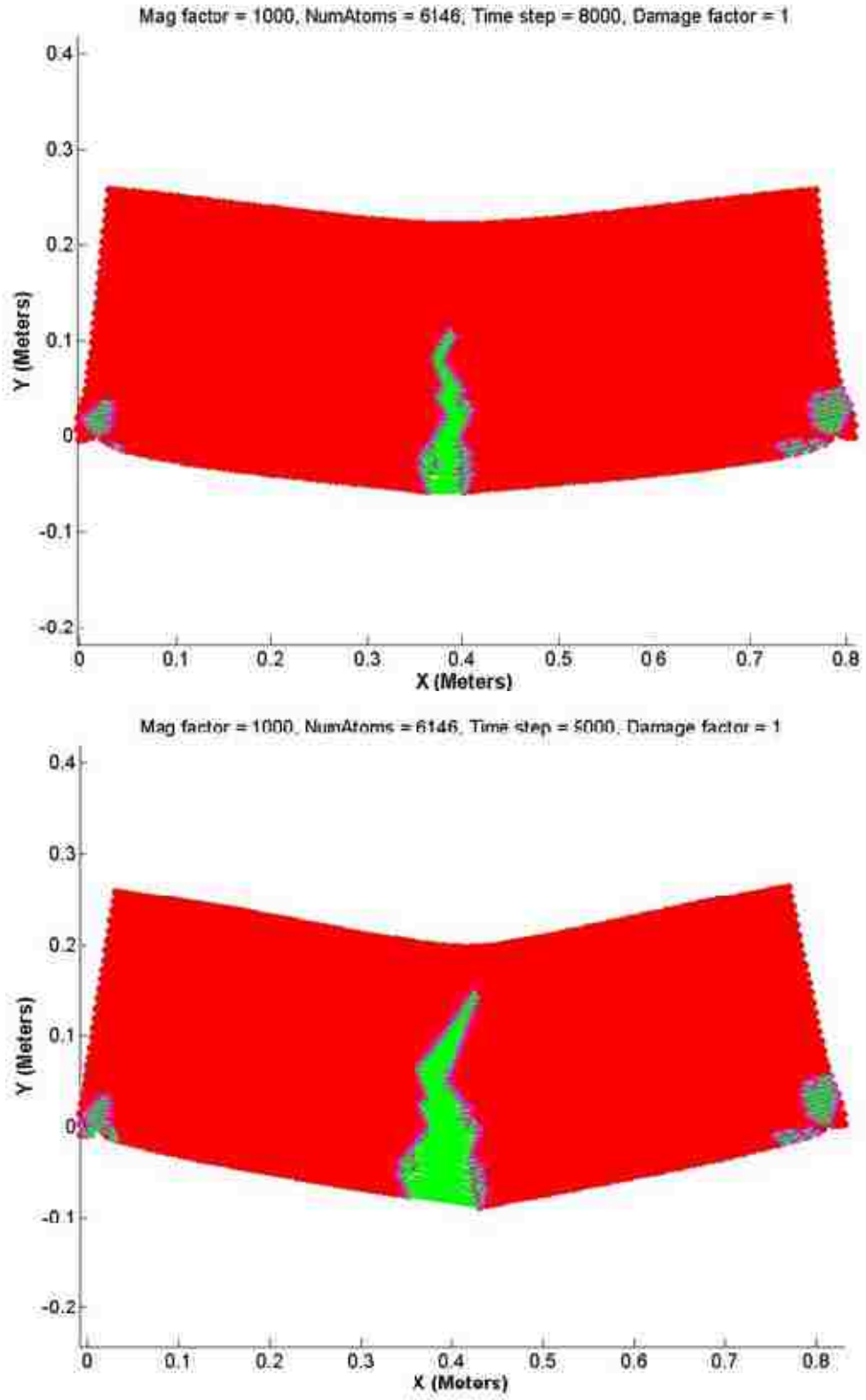

Fig. 5.4 Deformed shape of simply supported beam at (a) 8000 and (b) 9000 time steps, respectively.

5.2 Simply-supported reinforced concrete beam

A simply-supported reinforced concrete beam with seven half-inch diameter bars is simulated as shown in Fig. 5.5. We expect that this beam should fails in shear (due to flexure), as the reinforcement provided increases the flexural strength of the beam. Fig. 5.5 describes the beam that has been modeled for this example.

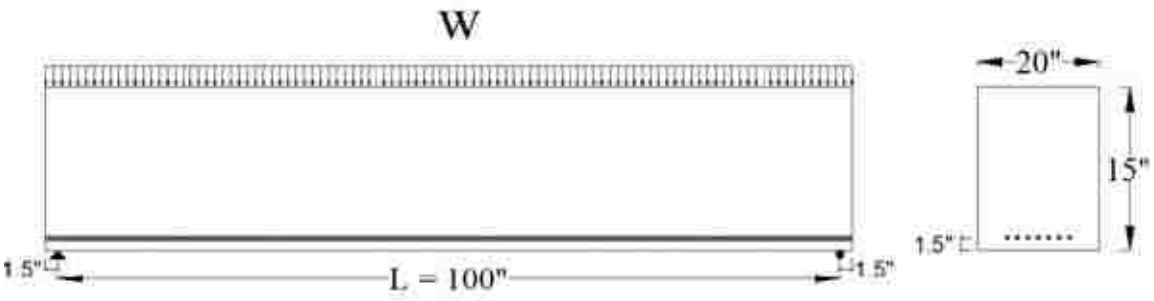

Fig. 5.5 Description of a simply supported reinforced concrete beam

Particle spacing is chosen to be one inch. The personal computer used in the previous problem is again used to run this simulation. It took about an hour to complete the simulation. Due to the addition of steel bars in the beam, the time step required to obtain a stable solution is reduced, and therefore the simulation time is increased.

The shear strength of the beam is calculated from the ACI shear specifications as

$$V_c = 2\lambda\sqrt{f_c'}b_w d, \tag{5.1}$$

where b_w is the width of the rectangular beam (20”), d is the effective depth of the beam (13.5”), $\lambda = 1$ for normal weight concrete, and f_c' is the compressive strength of the concrete at 28 days (4,000 psi)

The shear strength of the beam shown in Fig 5.5 is found to be 34.2 kips. The uniformly distributed load required to produce this shear is,

$$W = \frac{2V_c}{l} = 683 \text{ lb/in.} \tag{5.2}$$

A load of 700 lbs/in is applied on the beam shown in Fig. 5.3. The deformed shape of the beam is shown in Fig. 5.6.

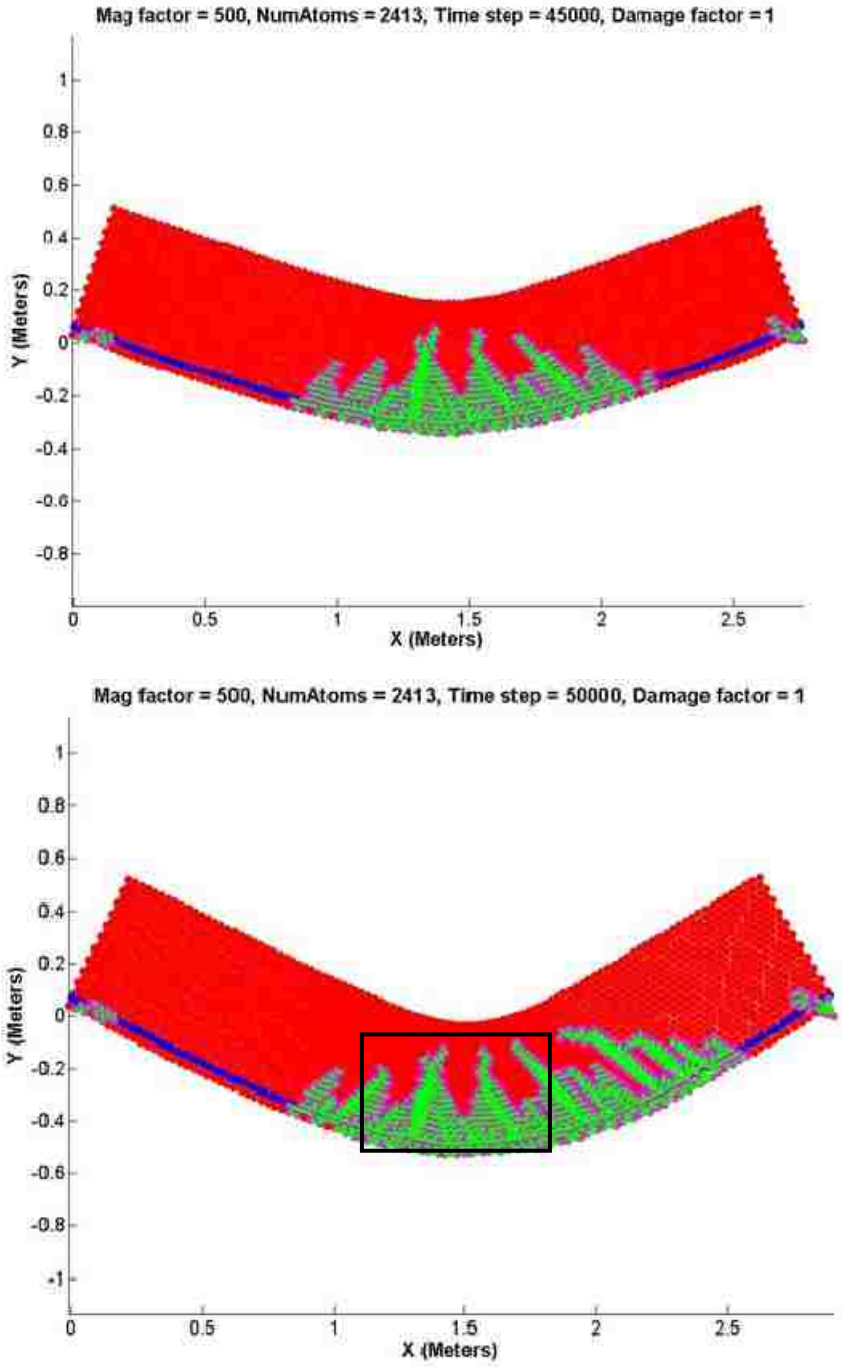

Fig. 5.6 Deformed shape of a reinforced simply supported at (a) 45,000, and (b) 50,000 time steps respectively.

Fig. 5.6 shows the deformed shape of a simply-supported reinforced concrete beam with damage and cracks. The green lines shown Fig. 5.6 represent the links that are broken in tension. There is distributed damage in the beam. If we closely observe the damage of the links as shown in Fig. 5.7 we see that the links that are damaged diagonally represent cracks and are branching as they grow. The horizontal lines are the cohesive damage of the link. This example demonstrates the flexural-shear cracking behavior of a reinforced concrete beam.

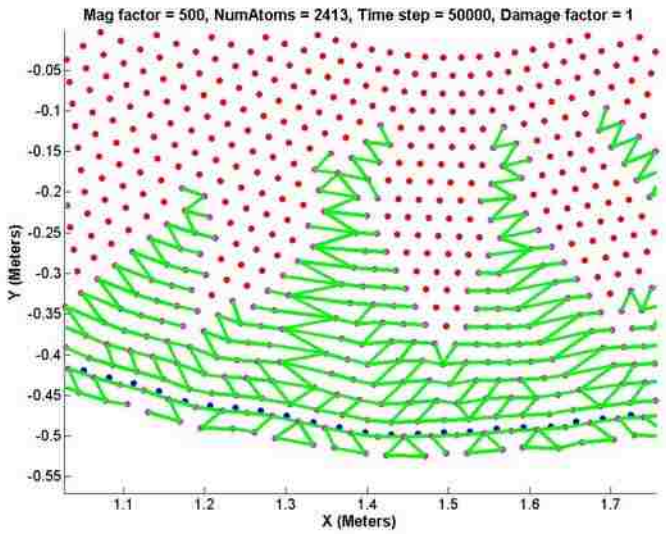

Fig. 5.7 Close view of the cracks shown in Fig 5.6 (b)

5.3 Unreinforced cantilever concrete beam

In this example, a 2D unreinforced cantilever beam is simulated. A fixed support is represented at the left end of the beam by restraining all the degrees of freedom of a column of particles. A concentrated load is applied to a column of particles at the free end of the beam. Fig 5.8 shows the description of the cantilever beam problem. This problem is simulated on a personal computer with a particle spacing of one inch. The simulation time for this problem is 27 minutes.

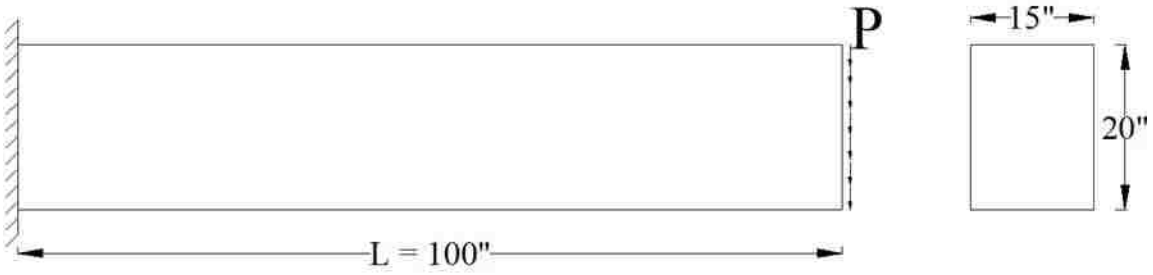

Fig. 5.8 Description of unreinforced cantilever concrete beam

The load, P, required for the beam shown in Fig. 5.8 for the tensile flexural crack to appear is found to be 2.5 kips. This load is equally distributed to all the 23 loaded particles on the right end of the beam. When a load of 2.5 kips is applied at the free end of the beam shown in Fig 5.8, the beam showed no sign of damage and a steady state solution was achieved. A load 2.7 kips is applied to observe the damage.

Fig. 5.9 shows the deformed shape of the beam with a crack. The ultimate load from pdQ and the analytical solution are comparable. This shows that the concrete model proposed in Chapter 3 and the calibrated material properties for the concrete model are reasonable.

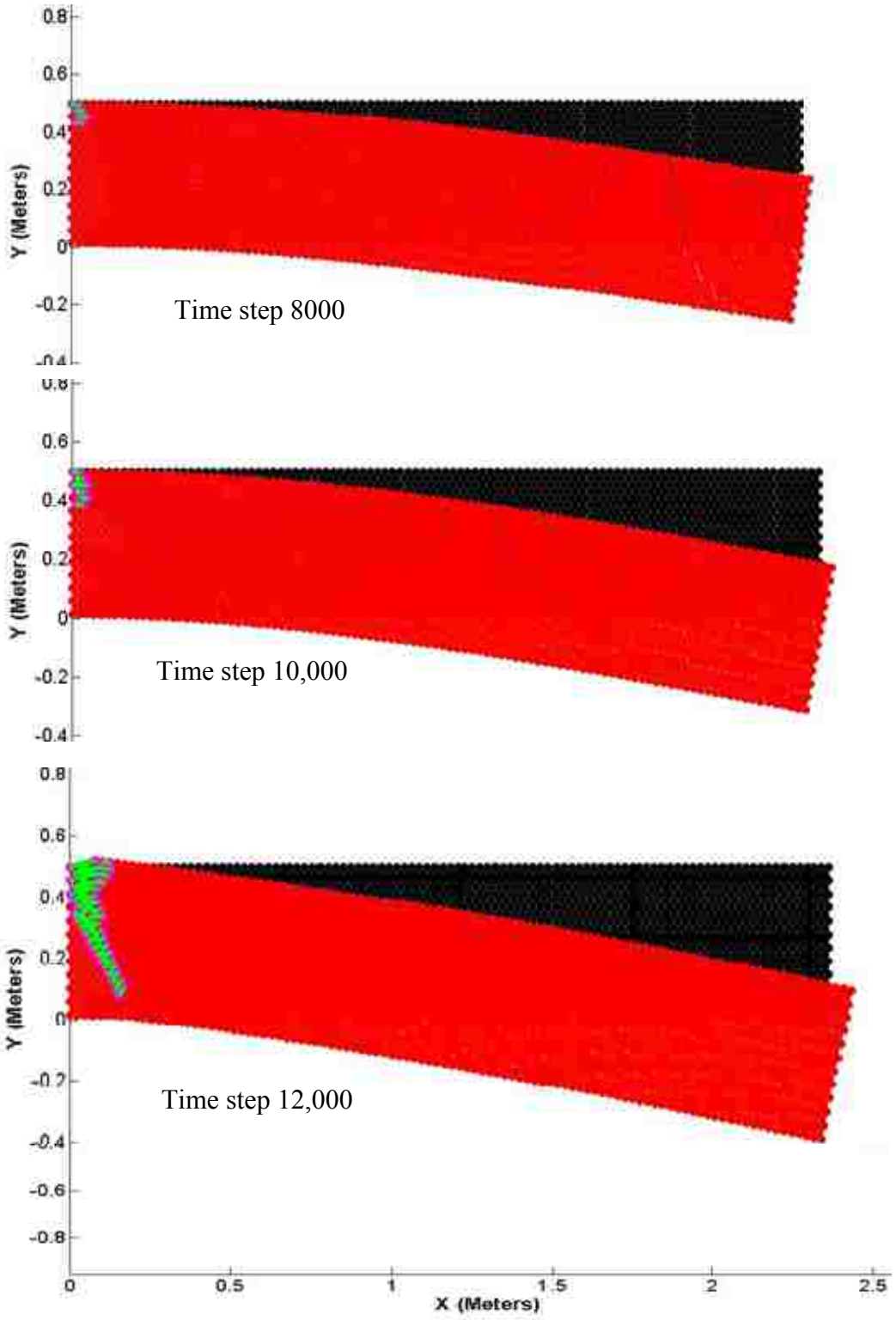

Fig. 5.9 Deformed shape of unreinforced cantilever beam

5.4 Reinforced cantilever concrete beam

This is the same problem as that of the previous cantilever beam but now it is reinforced with five steel bars of half-inch diameter in tension side at a distance of 1.5" from the top of the beam. Figure 5.10 shows the details of the beam model.

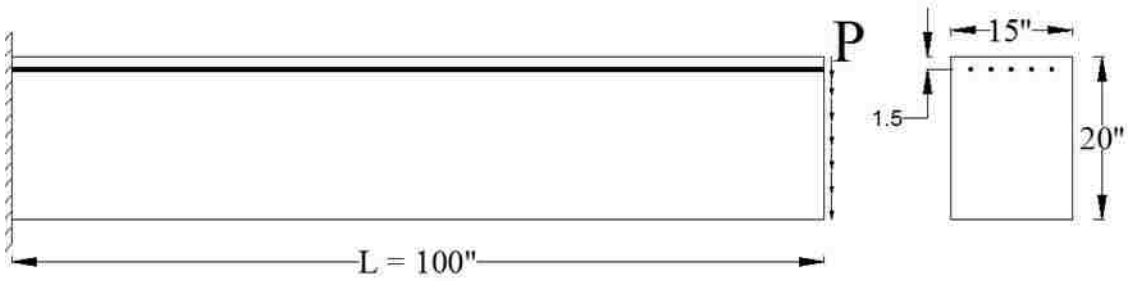

Fig. 5.10 Description of unreinforced cantilever concrete beam

This problem is simulated using the parallel version of pdQ. Four computing nodes with 16 processors are assigned to run this problem. The program took about 6 minutes to complete the simulation.

All the boundary conditions remain the same as in the previous problem. From ACI 318 the flexural and shear strength of the beam is found to be 10.35 kips and 37. 94 kips. It is clear from this that a flexural crack should start from the tension side of the beam.

A load of 7.5 kips is applied on the beam shown in Fig. 5.10. Fig. 5.11 shows the deformed shape of the reinforced cantilever beam. It is clear that the beam is failing in flexure. Crushing of the concrete particles can be noticed in the deformed shape of the beam with green color. The links that are failing in compression are represented by the green color.

The deformed beam shapes (red color) at different time steps are shown in Fig 5.11, the deformations are magnified by 50 times, the damage factor is 1, and the total number of particles is 2,121. In the Fig. 5.11, the deformed shape of the beam in shown twice in two columns at the same timestep. The figure to the left shows the deformed shape of the beam with the links that are broken. Blue color lines represent the links that are failed in tension, while the green color represents compressive broken links.

The reinforced cantilever beam example demonstrates the features of the concrete model. Reinforcement increases the flexural strength of the beam compared to unreinforced beam. It fails approximately at the same load that is calculated from the ACI code. Crushing of the concrete is observed after the steel yields.

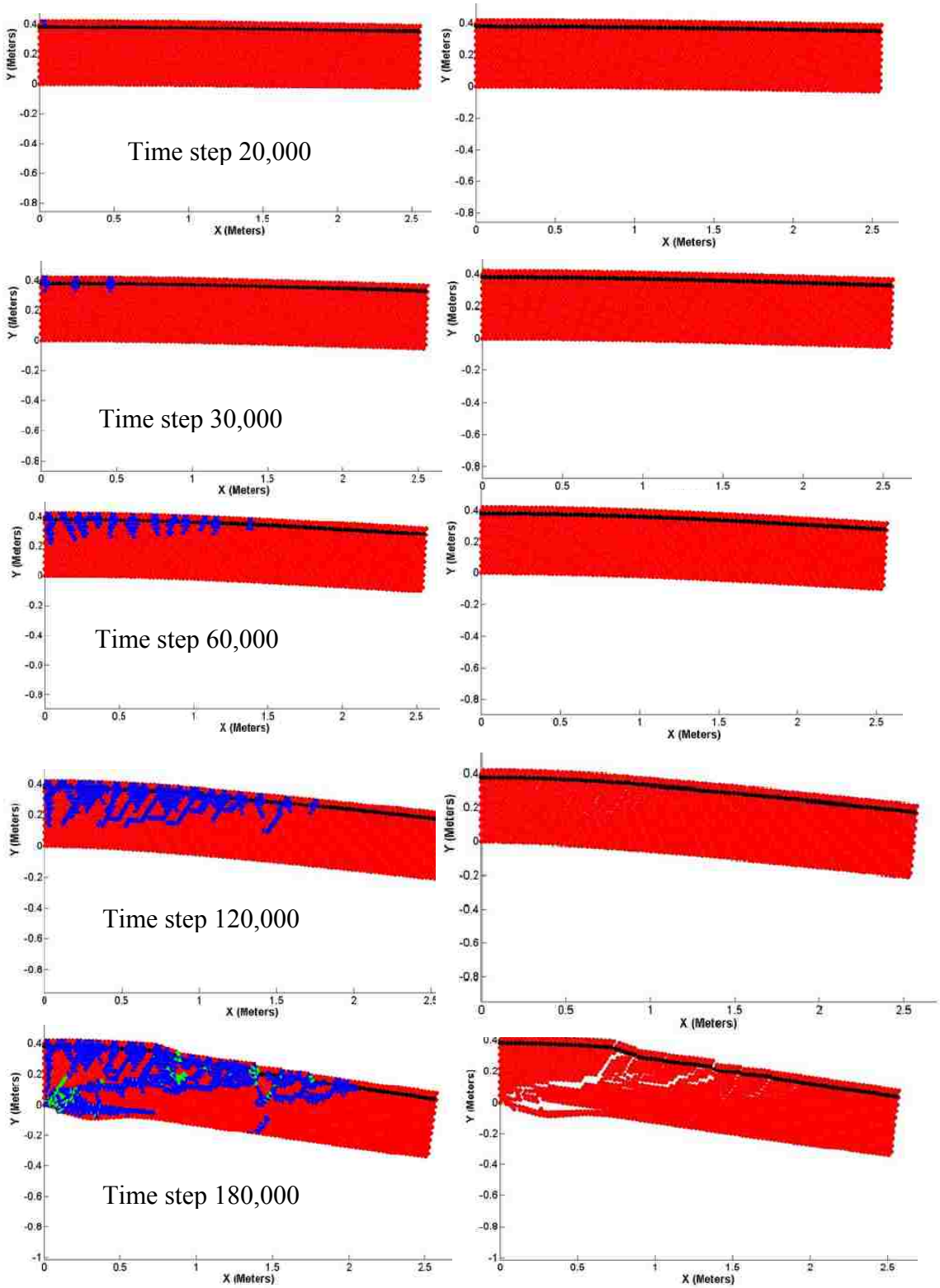

Fig. 5.11 Deformed shape of reinforced cantilever beam

5.4 Unreinforced concrete deep beam

A deep beam of length-to-depth ratio of two is simulated as shown in Fig. 5.12. It is expected that the deep beam with aspect ratio of 2 should fail in shear at supports. For this problem the spacing between the particles are kept to be one quarter of an inch. A uniformly distributed load is applied on the beam as shown in beam description.

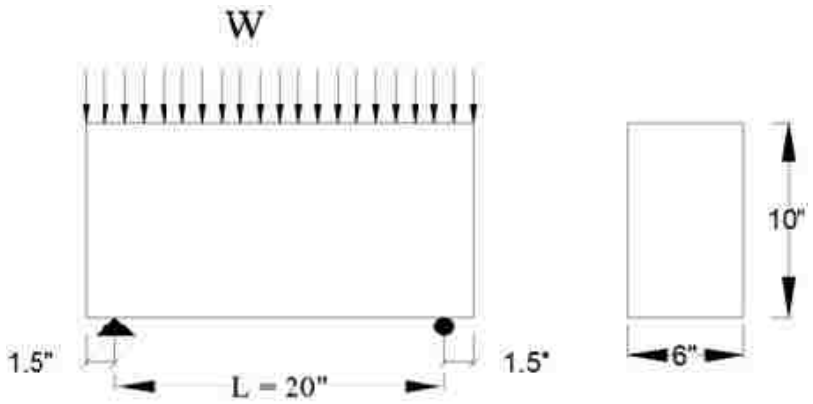

Fig. 5.12 Description of unreinforced concrete deep beam

According to ACI 318, the shear strength of the beam shown in Fig. 5.12 is found to be 75.8 kips. The uniformly distributed load required to produce the failure shear in the beam is found to be 7.58 kip/in. When a load of 4.75 kip/in is applied on the beam, the damage was observed with a small crack and then a static solution was achieved. A load of 5.00 kip/in is applied to observe the shear failure of the deep beam. Fig. 5.13 shows the deformed shape of the beam with shear failure. Cracks initiated near the supports where the shear is critical for deep beams. The deformed shape of the beam is plotted twice at the same time step. The figure on the left is plotted showing the links that failed. Blue-colored lines are the links that failed in tension, while the green-colored links represent links that failed in compression. The total number of particle is 3703. This problem is simulated using a machine with 8 processors. The time required to complete

the simulation is 4 minutes. Timestep is 8.39E-7 seconds. The deformations are magnified by 50x.

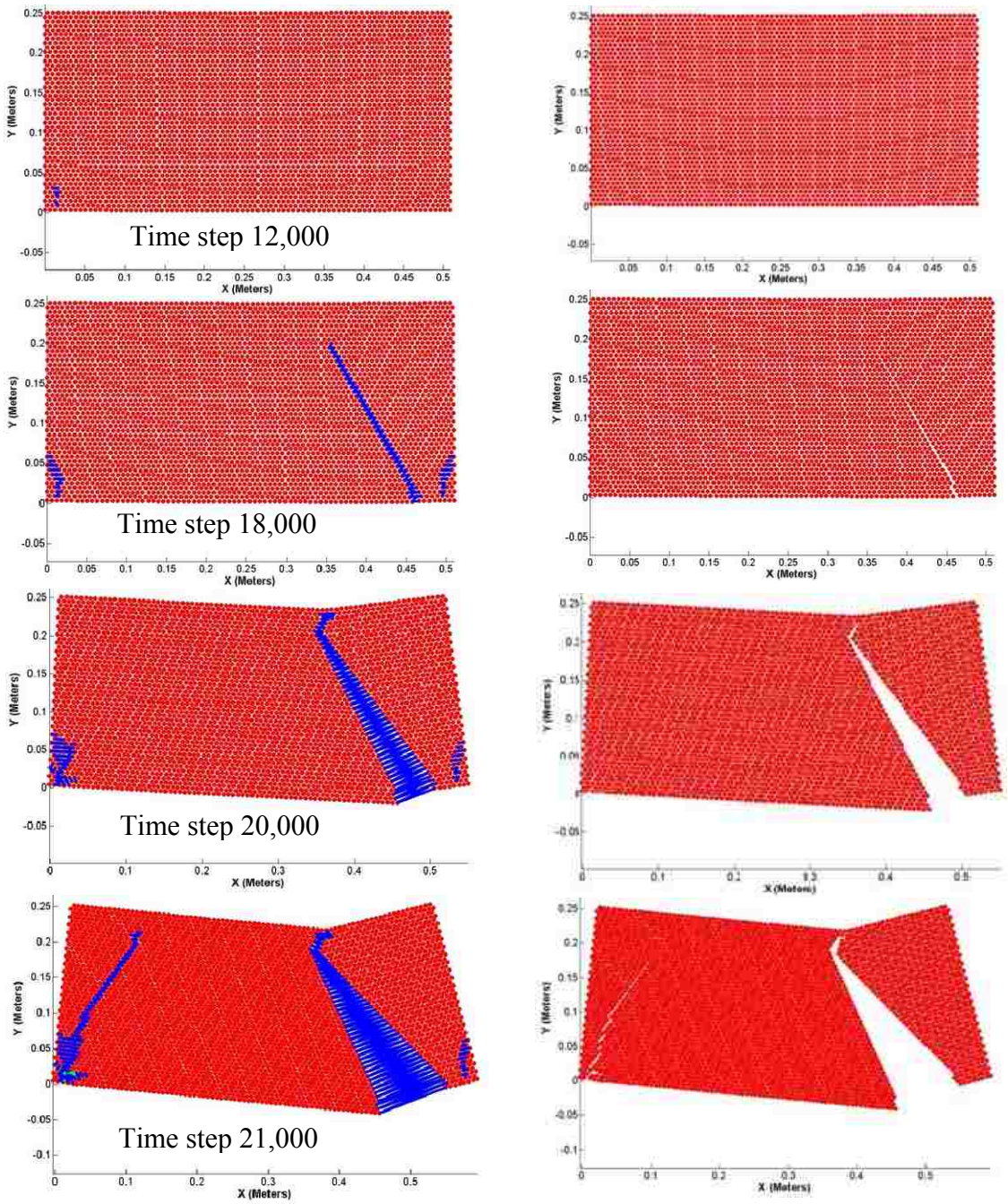

Fig. 5.13 Deformed shape of unreinforced deep beam

In this chapter, example problems were simulated to demonstrate the micropolar, state-based, lattice-based peridynamic concrete model proposed in this thesis. All the examples demonstrate the expected behavior of the beams. Though only a few benchmark problems were presented in this chapter, we can conclude that the model is capable of representing many of the most important features of concrete, including elasticity, damage and fracture. In the next chapter, we briefly summarize the work done in this thesis with conclusions drawn from these benchmark problems.

Chapter 6 Conclusions

In this chapter a brief summary of the work done in this thesis is presented. The conclusions are drawn based on the outcome of the results from the example problems.

6.1 Summary and conclusion.

The micropolar lattice-based, state-based peridynamic model (Fig. 6.1) presented in this thesis has the capability of modeling inelastic concrete damage. In the state-based model, the forces acting on the two particles no longer depend only on the states of the two particles, but they also depend on the states of the neighboring particles.

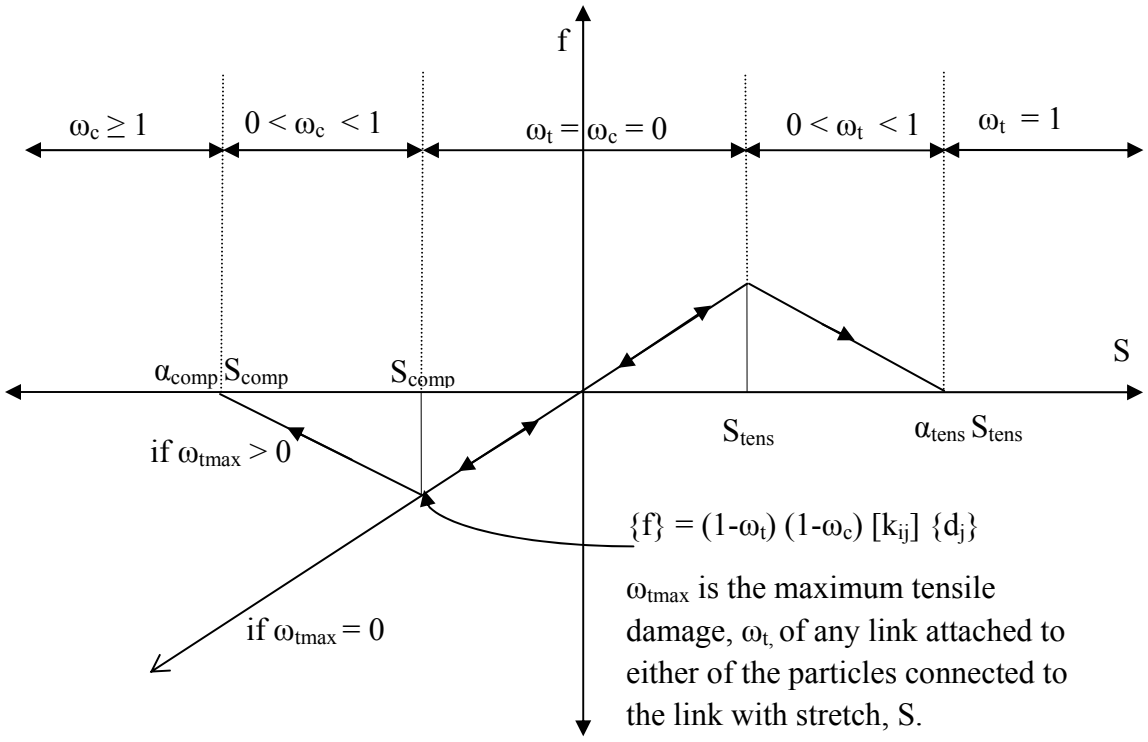

Fig. 6.1 Micropolar peridynamic damage model for concrete

In this micropolar, state-based, lattice-based peridynamic concrete model, we have introduced new damage parameters, (ω_c and ω_t). These damage parameters depend on the stretch in the link and evolve during the solution. The maximum values of the

damage parameters, (ω_c and ω_t), are 1 representing the complete damage of the link where the two particles no longer have a bond, and their minimum values are zero, representing linear elastic behavior. Unlike the previous concrete model in pdQ, once the link experiences damage, this damage increases progressively. The damage is irreversible.

In the linear elastic range of the stretch in the link, the forces and the stretch in the link can follow both directions as shown in Fig. 6.1. When the stretch in the link is in linear elastic and the particles are in dynamic motion, there can be reversal of the stretch which may increase or decrease.

The calibrated material parameters of the concrete model are shown to have reasonably replicated the features of concrete such as elasticity, damage, and fracture. Although 2D problems are simulated in this thesis as examples, the peridynamic micropolar model for concrete proposed in this thesis is also valid for 3D problems.

Although only the concrete model was defined and calibrated in this thesis, some example problems for a reinforced concrete beam are simulated. They show the capability of the model for a wide variety of problems. Shear cracks in reinforced concrete beams also show behavior similar to that seen in laboratory tests.

In this thesis we studied the sensitivity of the results with respect to the particle spacing. Although there is a small change in load at which first damage appears, the crack pattern is still consistent with the laboratory results, regardless of particle spacing.

In this implementation of micropolar, state-based, lattice-based peridynamic model for concrete we have the flexibility of modeling any quasi-brittle material (we define only a concrete model in this thesis) with any Poisson's ratio.

6.2 Future work.

Decent attempts have been made to fully represent the concrete by the micropolar state-based, lattice based model. This concrete model has still areas for improvement, as discussed below.

In this model the damage of the link, (ω_c and ω_t), is a function of the stretch in the link. Forces in the link are dependent on axial and flexural rigidities. ω_c or ω_t, should also probably depend on shear and bending deformations.

A better reinforced concrete bond model (steel-concrete particle interactions) can be developed. We have simplified the interactions between concrete and steel particles in this work (not considering the damage between concrete and steel particles). Better interaction models between them may improve model fidelity.

In this research we focused only on 2D problems; with some minor changes this concrete model can be used to simulate 3D problems.

References

Nguyen V. B., Chan A. H. C. and Crouch R. S. (2005). "Comparisons of Smeared Crack Models for RC Bridge Pier under Cyclic Loading", 13th ACME conference, University of Sheffield, pp. 111-114.

L Jendele, J.Cervenka, V. Saouma and R.Pukl 2001, "On the choice between discrete or smeared approach in practical structural FE analyses of concrete structures", 4th International Conference on Analysis of Discontinuous Deformation in Glasgow, Scotland UK, 6-8th June 2001

Silling S. 1998 "Reformulation of Elasticity Theory for Discontinuities and Long- Range Forces", Technical Report SAND98-2176, Sandia National Laboratories, Albuquerque, NM.

Sau N. 2008. "Peridynamic Modeling of Quasi-Brittle Structures", Ph.D.Dissertation, University of New Mexico, unpublished.

Gerstle W., Sau N. and Silling S. 2007. "Peridynamic Modeling of Concrete Structures", Nuclear Engineering and Design, 237(12-13): 1250-1258.

Gerstle W., Sau N. and Aguilera E. 2007 "Micropolar Peridynamic Constitutive Model for Concrete", 19th Intl. Conf. on Structural Mechanics in Reactor Technology (SMiRT 19), Toronto, Canada, August 12-17, B02/1-2.

Gerstle W. H., Sau N. and Aguilera E. 2007. "Micropolar Modeling of Concrete Structures", Proceedings of the 6th Intl. Conf. on Fracture Mechanics of Concrete Structures, Ia-FRAMCOS, Catania, Italy, June 17-22.

Gerstle W., Sau N. and Silling S. 2005. "Peridynamic Modeling of Plain and Reinforced Concrete Structures", Proceedings of the 18th Intl. Conf. on Structural Mechanics in Reactor Technology (SMiRT 18), Atomic Energy Press, Beijing China, Aug. 7-12, 949–956.

Gerstle W. H., Sau N. and Sakhavand N. 2009. "On Peridynamic Computational Simulation of Concrete Structures". Technical Report SP265-11, American Concrete Institute, 265: 245-264.

Gerstle W. and Sau N. 2004. "Peridynamic Modeling of Concrete Structures", Proceedings of the 5th Intl. Conf. on Fracture Mechanics of Concrete Structures, Li, Leung, Willam, and Billington, Eds., Ia-FRAMCOS, Vail, CO, 2: 949-956.

Hrennikoff, A. 1941, "Solution of problems of elasticity by the framework method", J. Appl. Mech., A169

Hansen, A., Roux, S. and Hermann, H.J. 1989 “Rupture of central force lattice”, J. Phys. France, 50, 733

Hansen, H., Roux, S. and Hermann, H.J. 1989, “Fracture of disordered. Elastic lattices in two dimensions”, Phsy. Rev B, 39, 637

Schlangen, E and Van Mier, J.G.M 1991, “Lattice model for numerical simulation of concrete fracture” in Proceedings Int’l Conference on Dam Fracture, Saouma, V.E., Dungar, R. and Morris, D., Eds., University of Colorado, Boulder, Sept. 11-13, 1991, Electric Power Research Institute, Palo Alto, CA, 511

Schlangen, E. and Vam Mier, J.G.M 1995, “Crack propagation in sandstone: A combined experimental and numerical approach”, Rock Mech. Rock Eng., 28(2), 93

Burt, N.J. and Dougil, J.W. 1997 Progressive failure in a model heterogeneous medium, J. Eng. Mech. Div. (ASCE), 103, 365

Zubelewicz, A and Bazant, Z.P 1987, Interface element modeling of fracture in aggregate composites, J. Eng. Mech. (ASCE), 113, 1619

Bazant, Z.P., Tabbara, M.R., Kazemi, M.T. and Pijaudier-Cabot, G. 1990, Random particle model for fracture of aggregate or fiber composites, J. Eng. Mech. (ASCE), 116, 1686

Daryl L. Logan 2011, A text on “A First Course in the Finite Element Method” fifth edition, CL-Engineering.

Hill, R. 1983, The mathematic theory of plasticity, Oxford University Press Editors.

Spencer, G.C. 1968 Introduction to plasticity, Chapman and Hall LTD Editors.

Mendelson A.1968. Plasticity: Theory and application. The Macmillan Company, Fred Landis Editor.

Jaroslav Kruis and Petr Stemberk, 2005. Fuzzyfication Of Chen Model Of Plasticity Of Concrete., VIII International Conference on Computational Plasticity COMPLAS VIII, Barcelona, 2005

Southwell., R.V., 1946, “Relaxation methods in Theoretical Physics.”, Oxford University Press.

W J Lewis, Tension Structures: Form and behaviour, London, Telford, 2003

Yun, Y. M., and Ramirez, J. A. “Strength of Struts and Nodes in Strut-and-Tie Model.” Journal
of Structural Engineering. V. 122, No. 1, January, 1996, pp 20-29.

ACI, 1997 Cracking Of Concrete Members in Direct Tension. Reported by American Concrete Institute (ACI) committee 224.

Huang Dan, Zhang Qing and Qiao Pizhong. March, 2011. "Damage and progressive failure of concrete structures using non-local peridynamic modeling", Science China Technological Sciences, Vol.54 No.3: pp 591–596.

Surendra P. Shah, Stuart E. Swartz and Chengsheng Ouyang 1995 "Fracture Mechanics of Concrete", John Wiley & Sons, Inc

Technical report on "Testing Compressive Strength of Concrete" by National Ready Mixed Concrete Association 2003, www.nrmca.org

Rahman A, 2012, Master's Thesis, "Lattice-based Peridynamic Modeling of Linear Elastic Solids", University of New Mexico, Albuquerque, NM.

Sakhavand N, 2011, Master's Thesis, "Parallel Simulation of Reinforced Concrete Structures Using Peridynamics", University of New Mexico, Albuquerque, NM.